Inorganic Chemistry

Article

pubs.acs.org/IC

Electronic Structure and Biologically Relevant Reactivity of Low-Spin {FeNO}^{8} Porphyrin Model Complexes: New Insight from a Bis-Picket Fence Porphyrin

Lauren E. Goodrich,[†] Saikat Roy,[†] E. Ercan Alp,[‡] Jiyong Zhao,[‡] Michael Y. Hu,[‡] and Nicolai Lehnert*[,†]

[†]Department of Chemistry, University of Michigan, Ann Arbor, Michigan 48109, United States

[‡]Advanced Photon Source, Argonne National Laboratory, Argonne, Illinois 60439, United States

Supporting Information

ABSTRACT: Because of HNO's emerging role as an important effector molecule in biology, there is great current interest in the coordination chemistry of HNO and its deprotonated form, the nitroxyl anion (NO^-), with hemes. Here we report the preparation of four new ferrous heme-nitroxyl model complexes, {FeNO}^{8} in the Enemark–Feltham notation, using three electron-poor porphyrin ligands and the bis-picket fence porphyrin H_2[3,5-Me-BAFP] (3,5-Me-BAFP^{2-} = 3,5-methyl-bis(aryloxy)-fence porphyrin dianion). Electrochemical reduction of [Fe(3,5-Me-BAFP)(NO)] (**1-NO**) induces a shift of ν(N–O) from 1684 to 1466 cm^{-1}, indicative of formation of $[Fe(3,5\text{-Me-BAFP})(NO)]^-$ (**1-NO**$^-$), and similar results are obtained with the electron-poor hemes. These results provide the basis to analyze general trends in the properties of ferrous heme-nitroxyl complexes for the first time. In particular, we found a strong correlation between the electronic structures of analogous {FeNO}^{7} and {FeNO}^{8} complexes, which we analyzed using density functional theory (DFT) calculations. To further study their reactivity, we have developed a new method for the preparation of bulk material of pure heme {FeNO}^{8} complexes via corresponding [Fe(porphyrin)]$^-$ species. Reaction of [Fe(T*o*-F_2PP)(NO)]$^-$ (T*o*-F_2PP^{2-} = tetra(*ortho*-difluorophenyl)porphyrin dianion) prepared this way with acetic acid generates the corresponding {FeNO}^{7} complex along with the release of H_2. Importantly, this disproportionation can be suppressed when the bis-picket fence porphyrin complex $[Fe(3,5\text{-Me-BAFP})(NO)]^-$ is used, and excitingly, with this system we were able to generate the first ferrous heme-NHO model complex reported to date. The picket fence of the porphyrin renders this HNO complex very stable, with a half-life of ~5 h at room temperature in solution. Finally, with analogous {FeNO}^{8} and {FeNHO}^{8} complexes in hand, their biologically relevant reactivity toward NO was then explored.

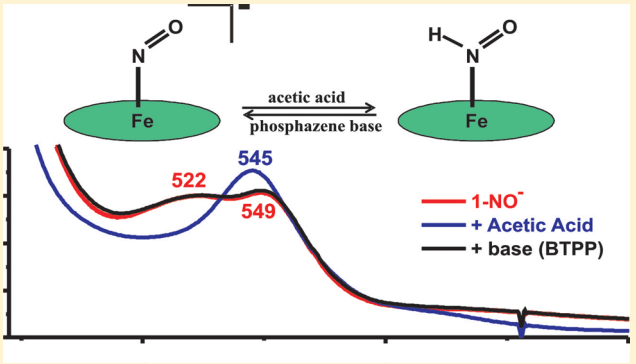

1. INTRODUCTION

Nitric oxide (NO) is toxic to cells at relatively low (μM) concentrations,[1] and it was therefore surprising when it was discovered in the 1980s that this diatomic is actually a signaling molecule in mammals at nM concentrations. In addition, macrophages produce NO at higher (local) concentration for the purpose of immune defense.[2−5] Because of its toxicity, both the biosynthesis of this molecule and its degradation are tightly regulated in mammalian organisms to prevent cellular damage. In denitrifying fungi that reduce nitrate to nitrous oxide (N_2O) for anaerobic respiration, the toxic metabolite NO is removed from the cell by the heme enzyme Cytochrome P450 nitric oxide reductase (P450nor) which catalyzes the reaction:[6,7] 2 NO + NAD(P)H + H^+ → N_2O + H_2O. In this case, a ferric nitrosyl intermediate is formed first,[8,9] which is then reduced by NAD(P)H in a two-electron process to form a ferrous nitroxyl (NO^- or HNO in aqueous environments) intermediate,[10] an {FeNO}^{8} or {FeNHO}^{8} complex in the Enemark–Feltham notation.[11] From stopped flow measurements on P450nor, this "Intermediate I", obtained upon reaction of the initial Fe(III)-NO adduct with NAD(P)H, is characterized by a Soret band absorption at 444 nm[10] and Fe-NO stretching frequency of 543 cm^{-1}.[12] Reaction with a second equivalent of NO then produces N_2O and closes the catalytic cycle. Density functional theory (DFT) and quantum mechanics/molecular mechanics (QM/MM) calculations[13,14] support the idea that the direct hydride transfer from NAD(P)H to the ferric nitrosyl complex generates a corresponding Fe(II)-NHO species, which could react directly with the second NO molecule. Alternatively, the Fe(II)-NHO complex could undergo protonation to a formally Fe(IV)-NHOH(-) (or Fe(III)-NHOH(radical)) structure prior to reaction with the second equivalent of NO. The computational results in fact predict that the Fe(II)-HNO species is basic because of the presence of the axial cysteinate ligand and, thus, will be easily protonated,[13,14] but experimental insight into

Received: April 19, 2013

 © XXXX American Chemical Society dx.doi.org/10.1021/ic400977h | *Inorg. Chem.* XXXX, XXX, XXX–XXX

this issue is lacking. So despite all of these studies, *the key question remains whether the nitroxyl intermediate of P450nor (Intermediate I) is singly or doubly protonated and what the significance of the protonation state is for the reactivity of this species with NO*. Without ferrous heme-nitroxyl model complexes in hand, this is difficult to ascertain because of our inability to precisely control protons, and proton dependent reactions, in protein (aqueous) environments.

Ferrous nitroxyl intermediates have also been proposed in the catalytic cycle of bacterial nitric oxide reductase (NorBC). NorBC, like P450nor, reduces two equivalents of NO to N_2O, but instead of a single heme active site as found in P450nor, NorBC contains a bimetallic heme/non-heme active site.[15] While the exact mechanism of NO reduction by NorBC is not known, one proposal (the "*cis*-heme b_3" mechanism) suggests that all of the NO chemistry happens exclusively at the heme b_3 site.[16] The *cis*-heme b_3 mechanism proposes that NO first binds the heme b_3 to form a ferrous heme-nitrosyl. A recent DFT paper indicates that reduction of this species to generate an $\{FeNO\}^8$ complex is crucial for the following reaction with NO to form the N−N bond and create a hyponitrite-level intermediate.[17] As there is currently no experimental evidence to support the key N−N bond forming step of this hypothesis, elucidation of the reaction of free NO with Fe(II)-NO^- complexes is of key importance to further validate the chemical basis for this mechanism.

In summary, mechanistic proposals have been put forth for both P450nor and NorBC where heme-bound nitroxyl intermediates of type $\{FeN(H_n)O\}^8$ (n = 0−2) react with NO. To systematically evaluate this proposed reactivity as a function of the protonation state of the $\{FeNO\}^8$ intermediate, model complexes are required that allow for a precise control of the proton (acid) concentration in solution. The most suitable approach to generate Fe(II)-nitroxyl model complexes is to start from a stable ferrous heme-nitrosyl adduct $\{FeNO\}^7$. The $\{FeNO\}^7$ precursor can be reduced by one-electron to an $\{FeNO\}^8$ species or ferrous nitroxyl complex, which could subsequently be protonated to generate the $\{FeNHO\}^8$ species. Initial studies by Kadish and co-workers demonstrated reversible one-electron reduction of five-coordinate ferrous heme-nitrosyls, utilizing TPP^{2-} and OEP^{2-} ligands, to generate Fe(II)-NO^- species as shown by UV−vis spectroelectrochemistry.[18,19] Ryan and co-workers provided further vibrational characterization of both $[Fe(TPP)(NO)]^-$ and $[Fe(OEP)(NO)]^-$.[20,21] Finally, using an extremely electron-poor porphyrin, $H_2TFPPBr_8$, Doctorovich and co-workers have isolated and characterized the corresponding five-coordinate Fe(II)-NO^- complex, obtained by reduction of the Fe(II)-NO starting material by cobaltocene.[22] Unfortunately, no reactivity of these complexes with NO has been reported, and all attempts at protonation of the formed Fe(II)-NO^- species to form a Fe(II)-HNO complex have resulted in regeneration of the corresponding Fe(II)-NO complex, presumably via disproportionation of an intermediately formed HNO adduct.[20,22] Ryan and co-workers also reported H_2 generation during this process.[20] No other details about the reactivity of these species are known, and because only very few $\{FeNO\}^8$ porphyrin model complexes have been prepared to date, their electronic structures are not well understood. Note that the only well characterized ferrous HNO complexes known to date were prepared by Farmer and co-workers in the myoglobin active site, and with human, soy and clam hemoglobin.[23,24]

In this paper, we report the spectroscopic and electronic-structural properties of four new $\{FeNO\}^8$ porphyrin complexes prepared either through the one-electron reduction of their $\{FeNO\}^7$ precursors or through corresponding $[Fe(porphyrin)]^-$ species, which is advantageous for the preparation of pure bulk material. This new library of $\{FeNO\}^8$ model complexes with different porphyrin ligands allowed us to establish a close correlation of the vibrational properties of the $\{FeNO\}^8$ complexes and their $\{FeNO\}^7$ precursors, demonstrating for the first time that their electronic structures are closely related. These results are further analyzed using DFT calculations. The $\{FeNO\}^8$ complexes were then investigated for reactivity toward (a) NO gas and (b) weak acids to generate HNO complexes. Application of the new bis-picket fence porphyrin 5,10,15,20-tetrakis(2,6-bis(3,5-dimethylphenoxy)phenyl) porphyrin, H_2[3,5-Me-BAFP], allowed for a breakthrough in these reactivity studies, as the bulky picket fence of this porphyrin efficiently prevented the previously observed disproportionation of the putative HNO adduct and intermolecular cross-reactions with NO. In particular, our results indicate a dramatic stabilization of heme-bound HNO with the new picket-fence porphyrin compared to the simple TPP^{2-} and OEP^{2-} ligands reported previously. Finally, initial results with respect to the biologically relevant reactivity of $\{FeN(H)O\}^8$ complexes with NO are reported that shine some light on proposed mechanisms for NO reductases.

2. EXPERIMENTAL SECTION

Synthesis. All reactions (except when noted otherwise) were performed under an inert gas atmosphere using dried and distilled solvents. Handling of air-sensitive samples was carried out under an N_2 atmosphere in an MBraun glovebox equipped with a circulating purifier (O_2, H_2O <0.1 ppm). Nitric oxide gas (Cryogenic Gases Inc., 99.5%) was passed through ascarite and then through a cold trap at −80 °C prior to usage to remove higher nitrogen oxide impurities. Nitric oxide-$^{15}N^{18}O$ (Aldrich, 98% ^{15}N, 95% ^{18}O) was used without further purification. 1-methylimidazole (MI) was distilled and degassed prior to use. Phosphazene base, P_1-*t*Bu-tris(tetramethylene), and glacial acetic acid were purchased from Aldrich and freeze−pump−thawed prior to use. Ammonia analysis was carried out using the phenolate assay originally developed by Russel.[25,26]

Tetrakis-5,10,15,20-(*per*-pentafluorophenyl)porphyrin, H_2[T*per*-F_5PP], and tetrakis-5,10,15,20-(*o*-difluorophenyl)porphyrin, H_2[T*o*-F_2PP], were synthesized and purified as previously reported.[27,28] Tetrakis-5,10,15,20-(2,6-dinitro-4-*tert*-butylphenyl)porphyrin, H_2[T*o*-$(NO_2)_2$-*p*-*t*BuPP], was prepared by BF_3−OEt catalyzed condensation of 2,6-dinitro-4-*tert*-butylbenzaldehyde[29] and pyrrole in CH_2Cl_2 as reported previously.[30] The porphyrin ligand H_2[3,5-Me-BAFP] was prepared according to modified literature procedures as described below.[31,32] Iron(III) chloride porphyrin complexes were prepared from the porphyrin ligand and excess $FeCl_2$ in refluxing dimethylformamide (DMF)[33] or tetrahydrofuran (THF) (see below; as needed). Five-coordinate ferrous porphyrin nitrosyls were prepared by reductive nitrosylation of the corresponding iron(III) chloride complexes.[34] A representative procedure for iron insertion and reductive nitrosylation is provided below. [^{57}Fe(3,5-Me-BAFP)(NO)] and [^{57}Fe(3,5-Me-BAFP)($^{15}N^{18}O$)] for nuclear resonance vibrational spectroscopy (NRVS) measurements were prepared in the same manner as the unlabeled complexes using $^{57}FeCl_2$ for the initial metalation.[35]

2,6-Bis(3′,5′-dimethylphenoxy)benzaldehyde. A 3.4 g portion of potassium methoxide, 12.5 mL of dry benzene, and 6.1 g of 3,5-dimethylphenol (50 mmol) were added to a 100 mL Schlenk flask. The mixture was allowed to stir under Ar(g) for 1 h. After 1 h, benzene and methanol were removed via a Schlenk line. 12.5 mL of

dx.doi.org/10.1021/ic400977h | *Inorg. Chem.* XXXX, XXX, XXX−XXX

dry pyridine was added, and the mixture was brought to a reflux. Then, 3.2 g of 2,6-dibromobenzaldehyde[31] and 0.19 g of copper(I) chloride were added quickly to the mixture. The reaction was kept at reflux under Ar(g) for 17 h. After 17 h, the mixture was added to 37 mL of ice water, and conc. hydrochloric acid was added until the solution became acidic. The reaction mixture was extracted with 20 mL of CH_2Cl_2, and the organic layer was washed with H_2O, saturated aqueous $NaHCO_3$, and H_2O. The mixture was concentrated to an oil using a rotary evaporator. The oil was chromatographed twice on silica with CH_2Cl_2 as the eluent. The fractions containing the desired product were rotary evaporated to a light yellow solid. Yield: 2.301 g (55%). ^{1}H NMR (400 MHz, $CDCl_3$): 10.57 (s, 1H); 7.30 (t, 1H); 6.80 (s, 2H); 6.69 (s, 4H); 6.56 (d, 2H); 2.30 (s, 12H); see Supporting Information, Figure S29.

3,5-Methyl-Bis(Aryloxy)-FencePorphyrin, H_2[3,5-Me-BAFP].[32] A 1.135 g portion of 2,6-bis(3,5-dimethylphenoxy)-benzaldehyde, 325 mL of CH_2Cl_2, and 2.5 mL of absolute ethanol were placed in a 500 mL round-bottom flask (RBF) and sparged with Ar(g). A 0.25 mL portion of pyrrole was then added via syringe, and the solution was stirred for 5 min. Then, 0.16 mL of boron trifluoride diethyletherate was added via syringe, and the solution was stirred in the dark for 1 h at room temperature. After 1 h, 0.56 g of dichlorodicyano-benzoquinone and 0.16 mL of triethylamine were added, and the reaction was stirred for an additional hour. The reaction mixture was then evaporated to dryness, chromatographed on silica with 100% CH_2Cl_2, and the obtained solid was recrystallized from CH_2Cl_2/MeOH. Yield: 349 mg (27%). ^{1}H NMR (400 MHz, $CDCl_3$): 8.86 (s, 8H); 7.59 (t, 4H); 7.06 (d, 8H); 6.13 (s, 16H); 6.02 (s, 8H); 1.66 (s, 48H); −2.98 (s, 2H); see Supporting Information, Figure S30. LCT MS: m/z 1576.1 (M+1). UV−vis (CH_2Cl_2): 424, 517, 554, 593 nm.

[Fe(3,5-Me-BAFP)(Cl)]. A 270 mg portion of H_2[3,5-Me-BAFP] in 60 mL of dry THF was brought to a reflux. Once refluxing, 0.22 g of $FeCl_2$ was quickly added, and the reaction was allowed to reflux for 3 h. The solution was evaporated to dryness and the crude material chromatographed on silica with 100% CH_2Cl_2 (to remove free base porphyrin) and 98:2 CH_2Cl_2:MeOH to elute the ferric porphyrin. The product band was evaporated, the resulting solid was redissolved in CH_2Cl_2 and washed with ∼1 M HCl. The organic layer was first dried with Na_2SO_4, and the solvent was then removed under reduced pressure to yield a dark purple powder. Yield: 186 mg (66%). LCT MS: m/z 1629.8 (M-Cl). UV−vis (CH_2Cl_2): 374, 424, 510, 584, 667 nm.

[Fe(3,5-Me-BAFP)(NO)] (1-NO). A 325 mg portion of [Fe(3,5-Me-BAFP)(Cl)] was dissolved in 9 mL of CH_2Cl_2 and 0.9 mL of MeOH. The solution was exposed to excess NO(g) and stirred at room temperature for 30 min. The resulting nitrosyl complex was precipitated with the addition of 24 mL of MeOH and stored at −30 °C overnight. The resulting solid was filtered under inert atmosphere and dried for 2 min under reduced pressure. Yield: 253 mg (78%). FT-IR: ν(N−O) 1684 cm^{-1}. [Fe(3,5-Me-BAFP)(^{15}N^{18}O)] was prepared with ^{15}N^{18}O using the same procedure. FT-IR: ν(^{15}N−^{18}O) 1614 cm^{-1}. UV−vis (1,2-DCE): 413, 478, 554 nm. UV−vis (THF): 422 (ε = 78800 M^{-1} cm^{-1}), 479 (8480 M^{-1} cm^{-1}), 555 (5280 M^{-1} cm^{-1}) nm.

Crystallization of [Fe(3,5-Me-BAFP)(NO)]. In the glovebox, ∼2 mg [Fe(3,5-Me-BAFP)(NO)] was dissolved in 1 mL of THF and placed in a 7 mm glass tube. 5 mL of MeOH were carefully layered on the THF solution, and the setup was left under an inert atmosphere. After 8 days, crystals suitable for X-ray analysis were collected.

[Fe(3,5-Me-BAFP)]. A 600 mg portion of **1-Cl** was dissolved in 50 mL of CH_2Cl_2 and stirred with excess 4 M NaOH (aq.) for 5 h. The organic layer was washed with water twice, dried with sodium sulfate and evaporated to dryness to yield [Fe(3,5-Me-BAFP)(OH)]. [Fe(3,5-Me-BAFP)(OH)] was heated to 70 °C in 40 mL of dry, degassed toluene with 3 mL of ethanethiol under inert atmosphere. After 4 h, the reaction was evaporated to dryness via Schlenk line. The resulting solid was redissolved in a minimum volume of degassed toluene, layered with hexanes, and placed at −30 °C overnight to precipitate. The resulting bright purple solid was collected. Yield: 570 mg (97%). UV−vis (THF): 434 (ε = 130800 M^{-1} cm^{-1}), 550 (6600 M^{-1} cm^{-1}) nm.

Generation of 1-NO$^-$. *Soret Band Concentration.* Under inert atmosphere, ∼1 mg of [Fe(3,5-Me-BAFP)] was dissolved in 30 mL of 0.1 M TBAP in THF. Using a two compartment bulk electrolysis cell outfitted with a UV−visible dip (immersion) probe (described below), the sample was reduced at −1.9 V vs Ag wire to obtain [Fe(3,5-Me-BAFP)]$^-$ (**1**$^-$). The applied potential was turned off, and 100 μL NO(g) was added. Formation of **1-NO**$^-$ was monitored by UV−visible spectroscopy and, upon completion (∼2 min) the solution was sparged for 10 min with N_2(g) to remove all free NO.

Q-Band Concentration. Under inert atmosphere, 12 mg of [Fe(3,5-Me-BAFP)] was dissolved in 30 mL of 0.1 M TBAP in THF. Using a two compartment bulk electrolysis cell outfitted with a UV−visible dip (immersion) probe (described below), the sample was reduced at −1.9 V vs Ag wire to obtain [Fe(3,5-Me-BAFP)]$^-$ (**1**$^-$). The applied potential was turned off, and 2 mL of NO(g) was added. Formation of **1-NO**$^-$ was monitored by UV−visible spectroscopy and, upon completion (∼4 min), the solution was sparged for 10 min with N_2(g) to remove all free NO.

Generation of 2-NO$^-$. Under inert atmosphere, ∼1 mg of [Fe(T*o*-F_2PP)] was dissolved in 30 mL of 0.1 M TBAP in THF. Using a two compartment bulk electrolysis cell outfitted with a UV−visible dip (immersion) probe (described below), the sample was reduced at −1.6 V vs Ag wire to obtain [Fe(T*o*-F_2PP)]$^-$ (**2**$^-$).The applied potential was turned off, and 100 μL of NO(g) was added. Formation of **2-NO**$^-$ was monitored by UV−visible spectroscopy and, upon completion (∼4 min), the solution was sparged for 10 min with N_2(g) to remove all free NO.

Physical Measurements. Infrared spectra were obtained from KBr disks on a Perkin-Elmer BX spectrometer at room temperature. Resolution was set to 2 cm^{-1}. Proton magnetic resonance spectra were recorded on a Varian Inova 400 MHz instrument. Electronic absorption spectra were measured using an Analytical Jena Specord 600 instrument at room temperature. Electron paramagnetic resonance spectra were recorded on a Bruker X-band EMX spectrometer equipped with an Oxford Instruments liquid nitrogen cryostat. EPR spectra were typically obtained on frozen solutions using 20 mW microwave power and 100kHz field modulation with the amplitude set to 1 G. Sample concentrations employed were ∼1 mM. Nuclear resonance vibrational spectroscopy (NRVS) data were obtained as described previously[36] at beamline 3-ID-XOR of the Advanced Photon Source (APS) at Argonne National Laboratory. This beamline provides about 2.5 × 10^9 photons/sec in ∼1 meV bandwidth (= 8 cm^{-1}) at 14.4125 keV in a 0.5 mm (vertical) × 0.5 mm (horizontal) spot. Samples were loaded into 4 × 7 × 1 mm copper NRVS cells. The final spectra represent averages of 6 scans. The program Phoenix was used to convert the NRVS raw data to the Vibrational Density of States (VDOS).[37,38]

Cyclic voltammograms (CVs) were recorded with a CH instruments CHI660C electrochemical workstation using a three component system consisting of a platinum or glassy carbon working electrode, a platinum auxiliary electrode, and an Ag wire pseudoreference electrode. CVs were measured in 0.1 M tetrabutylammonium perchlorate (TBAP) solutions in THF or 1,2-dichloroethane. Potentials are reported vs the measured Fc/Fc$^+$ couple. IR spectroelectrochemistry (∼4 mM) was performed using a solution IR cell with CaF_2 windows as previously described.[21] Electrodes consist of an 8 × 10 mm Pt mesh (100 mesh, 99.9%, Aldrich) for the working, 3 × 10 mm Pt mesh for the counter, and Ag wire (0.1 mm diameter, 99.9%, Aldrich) as a pseudoreference electrode. UV−vis spectroelectrochemistry (∼0.5 mM) was performed in a OTTLE cell.[39] Electrodes consist of an 8 × 10 mm Pt mesh (100 mesh, 99.9%, Aldrich) for the working, 3 × 20 mm Pt mesh for the counter, and Ag wire (1 mm diameter, 99.9%, Aldrich) as a pseudoreference electrode. Bulk electrolysis (at mM porphyrin concentrations) was performed in a two compartment setup where the carbon felt working electrode and Ag wire reference electrode are separated from the carbon felt counter electrode by a fine frit. The counter electrode compartment contains solvent and electrolyte. Electrolyte (TBAP of $TBAPF_6$) was 0.1 M. All

dx.doi.org/10.1021/ic400977h | Inorg. Chem. XXXX, XXX, XXX−XXX

bulk electrolysis experiments were performed at room temperature in the glovebox (O_2 < 0.1 ppm).

X-ray crystallography measurements were performed on a Rigaku RAXIS SPIDER diffractometer with an imaging area detector using graphite monochromated Cu−Kα radiation (1.5406 Å). A red prism crystal of $C_{108}H_{92}O_9N_5Fe \times 0.5THF$ having approximate dimensions of 0.29 × 0.09 × 0.05 mm was mounted on a MitiGen cryoloop. The data collection was made at 95 K. The data were processed with SADABS. An empirical absorption correction was applied to the structure. The structure was solved and refined with the Bruker SHELXTL (vs 2008/3) software package. The non-hydrogen atoms were refined anisotropically, and the hydrogen atoms were refined using the riding model. See Supporting Information, Table S1 for crystallographic data and measurement parameters.

DFT Calculations. All geometry optimizations and frequency calculations were performed with the program package Gaussian 03[40] using the BP86[41,42] functional and TZVP[43,44] basis set. Molecular orbitals were obtained from B3LYP[42,45,46]/TZVP single point calculations on the BP86/TZVP optimized structures using ORCA.[47] In all Gaussian calculations, convergence was reached when the relative change in the density matrix between subsequent iterations was less than 1×10^{-8}. Molecular orbitals were plotted with the program orca_plot included in the ORCA package and visualized using GaussView.

Determination of Binding Constants. To quantify 1-methylimidazole (MI) binding to five-coordinate ferrous heme-nitrosyls, the binding constant can be calculated for the reaction:

$$[Fe(TPP^*)(NO)] + MI \rightleftarrows [Fe(TPP^*)(MI)(NO)] \quad (1)$$

where $TPP^{*(2-)}$ is a phenyl-substituted tetraphenylporphyrin derivative. The titration of MI against the five-coordinate complex **1-NO** was followed by UV−visible spectroscopy, see Supporting Information, Figure S19, and K_{eq} can then be calculated from the equation

$$[MI] = c_T \Delta\varepsilon \left[\frac{MI}{\Delta E}\right] - K_{eq}^{-1} \quad (2)$$

which was originally developed by Drago and co-workers.[48−50] Here, c_T corresponds to the total concentration of porphyrin complexes, $c_T = c(6C) + c(5C)$, $\Delta\varepsilon$ is the difference in extinction coefficients, $\Delta\varepsilon = \varepsilon(6C) - \varepsilon(5C)$, and 5C and 6C abbreviate the five- and six-coordinate complexes, respectively. UV−vis absorption measurements are performed at different concentrations of MI ([MI]) and the change in absorbance (ΔE) is measured. A plot of [MI] versus [MI]/ΔE then gives K_{eq}^{-1}.

3. RESULTS AND ANALYSIS

3.1. Preparation and Characterization of {FeNO}^{7} Complexes. [Fe(3,5-Me-BAFP)(NO)] (**1-NO**), a {FeNO}^{7} complex in the Enemark−Feltham notation,[11] was prepared by reductive nitrosylation of [Fe(3,5-Me-BAFP)(Cl)]. The identity of **1-NO** has been confirmed by X-ray crystallography at 95 K. The crystal structure shows two equivalent molecules, **A** and **B**, in the unit cell that differ marginally in their structural parameters. Figure 1 shows a side view of one of the two molecules. As listed in Table 1, the Fe−NO and N−O bond lengths (for molecule **A**) are 1.71 and 1.15 Å, respectively. The Fe−N−O angle is 146° and the Fe-atom is displaced from the heme plane by 0.35 Å toward NO, typical of five-coordinate ferrous heme-nitrosyls.[51] Additionally, the crystal structure clearly demonstrates that the eight phenoxy-groups of the bis-picket fence porphyrin do, in fact, create a sterically hindered binding pocket for axial ligands, NO derivatives in our case.

Interestingly, this is the first crystal structure of a five-coordinate ferrous heme-nitrosyl with a TPP^{2-} derivative as coligand that shows a *single conformation* of the Fe-NO unit. It has been shown previously by Scheidt and co-workers that at 293 K the NO unit in [Fe(TPP)(NO)] is disordered over eight

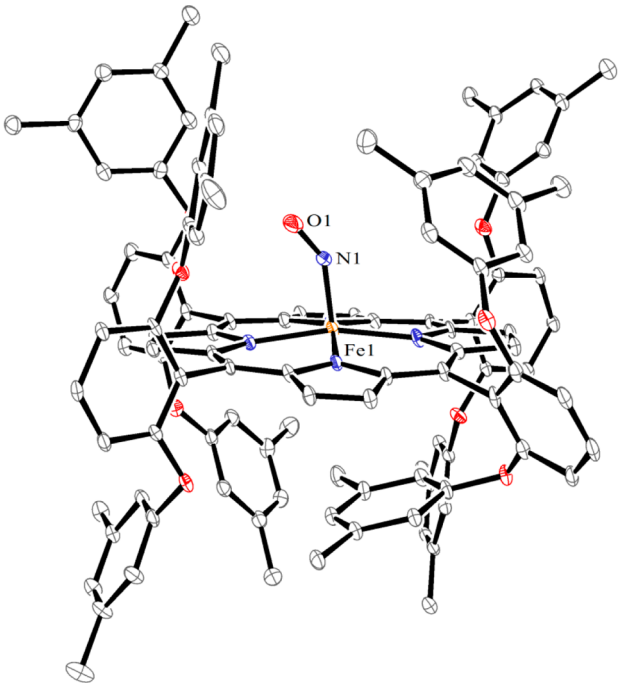

Figure 1. Crystal structure of [Fe(3,5-Me-BAFP)(NO)] (**1-NO**), hydrogen atoms are omitted for clarity. Key bond lengths and angles are provided in Table 1 and Supporting Information, Table S3. Thermal ellipsoids are shown at 30% probability.

possible positions (four on each side of the porphyrin plane).[34] Around 250 K, [Fe(TPP)(NO)] undergoes a phase transition from tetragonal to triclinic, and NO is now limited to two unique positions, one on each face of the porphyrin plane.[52] Excitingly, the eight phenoxy groups of the porphyrin ligand in **1-NO** direct packing of the molecules in the crystal in a way that further limits the Fe-NO unit to a single orientation (but note that the presence of a more disordered phase at high temperature cannot be ruled out). The steric encumbrance of this bulky porphyrin also appears to direct the position of NO relative to the Fe−$N_{pyrrole}$ bonds: in the case of **1-NO**, the N−O unit is located *directly above* one of the Fe−$N_{pyrrole}$ bonds. This is in contrast to other five-coordinate ferrous heme-nitrosyls where the O-atom is positioned toward a meso-carbon; for example, in [Fe(TPP)(NO)] the N−O unit is rotated 44° from the closest Fe−$N_{pyrrole}$ bond.[52] This difference results in a unique core asymmetry in **1-NO**. In this complex, the Fe−$N_{pyrrole}$ bond which is aligned with the N−O unit (1.969 Å) is significantly shorter than the remaining three bonds (1.997, 1.992, and 2.005 Å). Typically, when the N−O unit points toward a meso-carbon of the porphyrin ligand, two Fe−$N_{pyrrole}$ bonds are shorter (in the direction of NO) than the remaining two bonds.[53] In the case of [Fe(OEP)(NO)], the short Fe−$N_{pyrrole}$ bond lengths are 1.989 and 1.993 Å, and the long bonds are 2.017 and 2.016 Å.[54]

The {FeNO}^{7} complex **1-NO** shows an electron paramagnetic resonance (EPR) spectrum typical of a $S = 1/2$ five-coordinate ferrous heme-nitrosyl with g-values of 2.10, 2.06, and 2.01 in toluene (see Supporting Information, Figure S1). A well-defined 3-line hyperfine pattern is observed on the smallest g-value, g_z from the ^{14}N nuclear spin ($I = 1$) of bound NO. In THF, however, the three-line hyperfine on g_z begins to migrate toward g_y, indicating possible binding of THF at 77 K to form a six-coordinate nitrosyl with bound THF in solution. IR spectra

dx.doi.org/10.1021/ic400977h | Inorg. Chem. XXXX, XXX, XXX−XXX

Table 1. Crystallographic Parameters ([Å] and [deg]) of Selected Five-Coordinate Ferrous Porphyrin Nitrosyls

complex	T [K]	ΔFe−NO	ΔN−O	∠Fe−N−O	ΔFe−$N_{pyrrole}$	ΔFe−$N_{pyrrole}$[a]	ΔFe[b]	ref.
[Fe(3,5-Me-BAFP)(NO)] (**1-NO**), **A**	95	1.712	1.150	146.27	1.969	1.991(8)	0.35	*t.w.*[c]
					1.997			
					1.992			
					2.005			
[Fe(3,5-Me-BAFP)(**NO**)] (**1-NO**), **B**	95	1.714	1.142	146.52	1.975	1.993(5)	0.37	*t.w.*
					1.989			
					2.002			
					2.008			
[Fe(TPP)(NO)]	33	1.740	1.164	144.5		1.999	0.20	52
[Fe(TPP)(NO)]	293	1.721	1.107	149.6		2.001	0.23	52
[Fe(OEP)(NO)], **A**	130	1.722	1.167	144.4	1.989	2.004	0.29	54
					1.993			
					2.017			
					2.016			
[Fe(OEP)(NO)], **B**	130	1.731	1.168	142.7	2.000	2.010	0.27	54
					1.999			
					2.017			
					2.023			

[a]Average of all four Fe−$N_{pyrrole}$ bond lengths [b]Iron displacement from the 24 atom mean porphyrin plane [c]This work

in KBr show a clear nitric oxide stretching frequency, ν(N−O), of 1684 cm^{-1} which shifts to 1614 cm^{-1} upon $^{15}N^{18}O$ isotope labeling as shown in Supporting Information, Figure S2. Furthermore, utilizing nuclear resonance vibrational spectroscopy the Fe-NO stretching frequency, ν(Fe-NO), of **1-NO** is found at 518 cm^{-1} which shifts by 16 cm^{-1} to lower energy in **1-$^{15}N^{18}O$** (Supporting Information, Figure S3). The Fe−N−O bending mode is unable to be assigned because of noise in the **1-NO** spectrum and overlap with other Fe-centered vibrations in the 380 cm^{-1} region.

Three additional "electron-poor" {FeNO}^{7} porphyrin complexes have been synthesized for the purpose of this study. [Fe(T*o*-F_2PP)(NO)] (**2-NO**), [Fe(T*per*-F_5PP)(NO)] (**3-NO**), and [Fe(T*o*-$(NO_2)_2$-*p*-*t*BuPP)(NO)] (**4-NO**) all show typical N−O stretching frequencies for five-coordinate ferrous heme-nitrosyls (Table 2; 2-**NO** and 3-**NO** were previously reported, see ref 55). The ν(N−O) for **2-NO**, **3-NO**, and **4-NO** in a KBr matrix are 1687, 1699, and 1693 cm^{-1} respectively. EPR spectroscopy indicates that all three complexes are low-spin Fe(II)-NO species with S = 1/2 ground states. For **3-NO** and **4-NO**, the EPR spectrum shows the usual case where a well-defined three-line hyperfine pattern is observed on the smallest g-value, g_z, that stems from the ^{14}N nuclear spin (I = 1) of bound NO (Supporting Information, Figure S4; A_z = 47 MHz in both spectra). Interestingly, in the case of **2-NO**, this hyperfine interaction is now resolved on all three g-values. This is a unique case and correspondingly, the experimental spectrum and simulation generated using the program Spin Count are provided in Figure 2. The g-values are 2.11, 2.04, and 2.00—similar to both **3-NO**, **4-NO**, and other five-coordinate ferrous heme systems.[16] The hyperfine coupling constants for A_x, A_y, and A_z are 39, 46, and 47 MHz, respectively.

3.2. Spectroelectrochemical Reduction of Five-Coordinate Ferrous Heme-Nitrosyls. The cyclic voltammogram of **1-NO** shows a quasi-reversible reduction at −1.78 V vs Fc/Fc^+ in THF (Figure 3). This reduction potential is 310 and 190 mV more negative than those for the one-electron reduction of the previously characterized complexes [Fe(TPP)(NO)] and [Fe(OEP)(NO)], respectively (Table 3).[18,19] To characterize this reduction further, infrared spectroelectrochemical measurements were performed in thin layer cells. As shown in Figure 4, upon one-electron reduction of **1-NO** in 1,2-DCE-d_4 the ν(N−O) band at 1684 cm^{-1} of the {FeNO}^{7} starting complex decreases in intensity as a new band at ∼1466 cm^{-1} appears. While this N−O stretching vibration of the {FeNO}^{8} complex (**1-NO$^-$**) is partially masked by a porphyrin ligand band, $^{15}N^{18}O$ labeling shifts this band into an open window of the IR

Table 2. Fe-NO and N−O Stretching Frequencies of Selected Five- and Six-Coordinate {FeNO}^{7} and {FeNO}^{8} Iron Porphyrin Nitrosyls

complex	ν(N−O)	ν(Fe−NO)	ref.
{FeNO}^{7}			
five-coordinate			
[Fe(OEP)(NO)]	1671	522	60
[Fe(3,5-Me-BAFP)(NO)] (**1-NO**)	1684	518	*t.w.*
[Fe(T*o*-F_2TPP)(NO)] (**2-NO**)	1687		*t.w.*
[Fe(T*o*-$(NO_2)_2$-*p*-tBuPP)(NO)] (**4-NO**)	1693		*t.w.*
[Fe(TPP)(NO)]	1697	532	58
[Fe(T*per*-F_5TPP)(NO)] (**3-NO**)	1699		*t.w.*
[Fe(TFPPBr$_8$)(NO)]	1727		22
six-coordinate			
[Fe(3,5-Me-BAFP)(THF)(NO)] (**1_{THF}-NO**)	1661		*t.w.*
[Fe(3,5-Me-BAFP)(MI)(NO)] (**1_{MI}-NO**)	1630		*t.w.*
[Fe(T*o*-F_2TPP)(MI)(NO)] (**2_{MI}-NO**)	1636		*t.w.*
[Fe(T*o*-$(NO_2)_2$-*p*-tBuPP)(MI)(NO)] (**4_{MI}-NO**)	1641		*t.w.*
[Fe(TPP)(MI)(NO)]	1630	437	36,59
[Fe(T*per*-F_5TPP)(MI)(NO)] (**3_{MI}-NO**)	1649		*t.w.*
{FeNO}^{8}			
[Fe(OEP)(NO)]$^-$	1441		21
[Fe(3,5-Me-BAFP)(NO)]$^-$ (**1-NO$^-$**)	1466		*t.w.*
[Fe(T*o*-F_2PP)(NO)]$^-$ (**2-NO$^-$**)	1473		*t.w.*
[Fe(T*o*-$(NO_2)_2$-*p*-tBuPP)(NO)]$^-$ (**4-NO$^-$**)	1482		*t.w.*
[Fe(TPP)(NO)]$^-$	1496	549	20
[Fe(T*per*-F_5TPP)(NO)]$^-$ (**3-NO$^-$**)	∼1500		*t.w.*
[Fe(TFPPBr$_8$)(NO)]$^-$	1550		22

dx.doi.org/10.1021/ic400977h | *Inorg. Chem.* XXXX, XXX, XXX−XXX

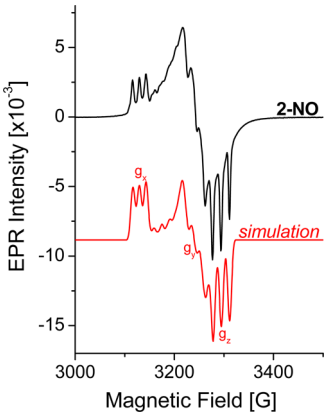

Figure 2. EPR spectrum of [Fe(T*o*-F_2PP)(NO)] (**2-NO**). The three-line hyperfine pattern on all g-values originates from the nuclear spin of the ^{14}N-atom (I = 1) of NO. The simulated spectrum was generated using the program SpinCount. Fit parameters are g_x = 2.109, g_y = 2.0375, g_z = 2.003, A_x = 39 MHz, A_y = 46 MHz, A_z = 47 MHz, sg_x (g-strain) = 0.0025, sg_y = 0.0035, and sg_z = 0.002.

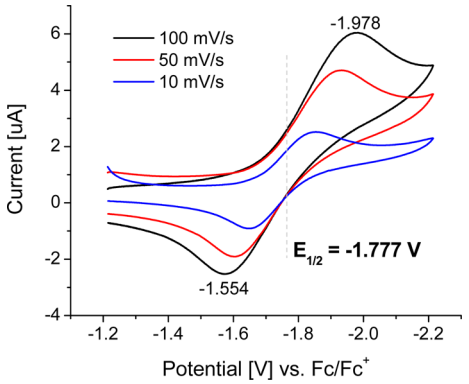

Figure 3. Cyclic voltammograms for [Fe(3,5-Me-BAFP)(NO)] (**1-NO**) in THF at various scan rates.

Table 3. Half Wave Potentials (in V vs. Fc/Fc$^+$) for the First Reduction of Ferrous Porphyrin Nitrosyls

complex	solvent	[Fe(P)(NO)]/[Fe(P)(NO)]$^-$	ref.
[Fe(OEP)(NO)]	CH_2Cl_2	−1.59	18
[Fe(3,5-Me-BAFP)(NO)] (**1-NO**)	THF	−1.78	*t.w.*
[Fe(T*o*-F_2TPP)(NO)] (**2-NO**)	1,2-DCE	−1.18	*t.w.*
[Fe(T*o*-$(NO_2)_2$-*p*-tBuPP)(NO)] (**4-NO**)	1,2-DCE	−1.18	*t.w.*
[Fe(TPP)(NO)]	CH_2Cl_2	−1.42	18
	THF	−1.47	18
[Fe(T*per*-F_5TPP)(NO)] (**3-NO**)	1,2-DCE	−1.13	*t.w.*
[Fe(TFPPBr_8)(NO)]	CH_2Cl_2	−0.65	22

spectrum at ∼1400 cm^{-1}. Importantly, this reduction is chemically completely reversible: upon reoxidation, as shown in Supporting Information, Figures S6 and S7, complex **1-NO** is regenerated. Natural abundance NO and ^{15}N^{18}O difference spectra for **1-NO** and **1-NO**$^-$ are provided in the Supporting Information, Figure S8, to further confirm the assignment of the N−O stretching frequency of **1-NO**$^-$.

As listed in Table 2, the ν(N−O) frequency of **1-NO**$^-$ is consistent with previously reported values for five-coordinate {FeNO}^{8} porphyrin systems, where ν(N−O) is observed between 1440−1550 cm^{-1}. In contrast, low-spin *non-heme* iron

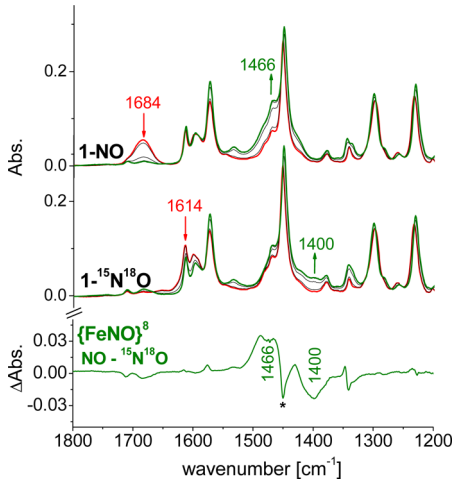

Figure 4. Infrared spectra for the spectroelectrochemical reduction of [Fe(3,5-Me-BAFP)(NO)] (top, **1-NO**) and [Fe(3,5-Me-BAFP)-(^{15}N^{18}O)] (middle, **1-^{15}N^{18}O**). Difference spectra are provided in Supporting Information, Figure S8. The asterisk (*) indicates poor subtraction of a porphyrin band at 1450 cm^{-1}. The estimated isotope shift (by DFT) of the N−O stretch in the NO$^-$ complex is 61 cm^{-1}, indicating that the 1450 cm^{-1} feature in the reduced compound is too high in energy to be the ν(^{15}N−^{18}O) stretch.

nitrosyls typically show significantly lower N−O stretching frequencies (∼1300 cm^{-1}). This suggests a strongly NO ligand-centered reduction for the low-spin non-heme NO adducts and a more metal based reduction for the heme systems. Previous DFT calculations from our group have shown that for the heme complexes this corresponds to an electronic structure that is intermediate between low-spin Fe(II)-NO$^-$ ↔ Fe(I)NO•.[13]

UV−visible spectroelectrochemical measurements in an OTTLE cell were used to further characterize the one electron reduced complex **1-NO**$^-$ as shown in Figure 5. As the potential is swept reductively from −0.4 V to −1.8 V vs Ag wire at 10 mV/s, there is essentially no change in the Soret band at 413 nm when 1,2-DCE is used as solvent, but dramatic changes are observed in the Q-band region (see Figure 5, top). The band at 478 nm decreases in intensity while a new band appears at 523 nm upon reduction. The clean isosbestic point at 504 nm is indicative of a clean conversion from **1-NO** to **1-NO**$^-$ without further intermediates. The spectral changes observed for the reduction of **1-NO** are in agreement with the reduction of [Fe(TPP)(NO)] reported previously.[20] Importantly, this does not correspond to a reduction of the porphyrin ligand, as this is accompanied by a dramatic loss of intensity of the Soret band not observed here. As an illustration of a porphyrin-centered reduction the spectroelectrochemical reduction of [Fe(3,5-Me-BAFP)] in THF is provided in the Supporting Information, Figure S11. For **1-NO**, this porphyrin reduction (corresponding to a two-electron reduction of the {FeNO}^{7} complex) is not accessible in 1,2-DCE.

Upon dissolving **1-NO** in THF, the Soret band shifts by 9 nm from 413 to 422 nm, indicating binding of THF in this system. Solution IR spectra support formation of [Fe(3,5-Me-BAFP)(NO)(THF)] with a new ν(N−O) band at 1661 cm^{-1}. Additionally, the EPR spectrum of **1-NO** in THF indicates weak binding of THF as discussed above (Supporting Information, Figure S1). However, upon one-electron reduction of this species (Figure 5, bottom), the resulting spectrum overlays perfectly with the data obtained for the reduction of

dx.doi.org/10.1021/ic400977h | *Inorg. Chem.* XXXX, XXX, XXX−XXX

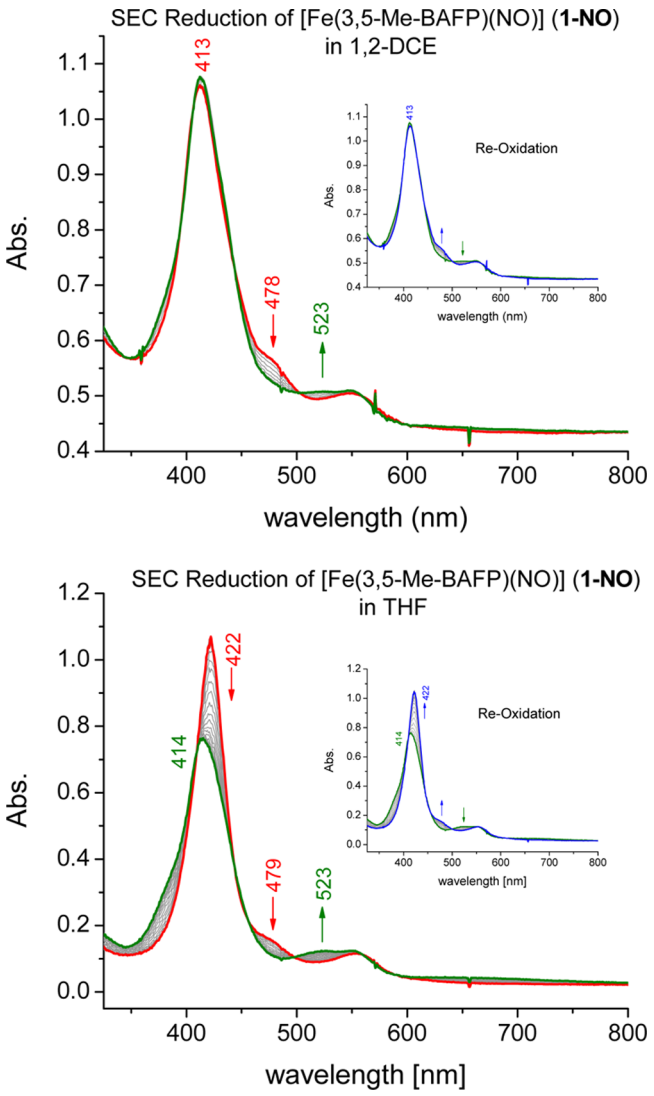

Figure 5. UV−visible absorption spectra for the spectroelectrochemical reduction of [Fe(3,5-Me-BAFP)(NO)] (**1-NO**, red to green), obtained by sweeping from −0.4 V to −1.8 V vs Ag wire at a rate of 10 mV/s in a 0.1 M TBAP solution in dry (top) 1,2-DCE and (bottom) THF. The reaction is chemically completely reversible upon sweeping from −1.8 V to −0.4 V vs Ag wire (inset).

five-coordinate **1-NO** in 1,2-DCE. This strongly suggests that the reduction product of six-coordinate [Fe(3,5-Me-BAFP)(NO)(THF)] is five-coordinate [Fe(3,5-Me-BAFP)(NO)]$^-$ (**1-NO**$^-$). As such, this indicates that the thermodynamic *σ-trans* effect of NO$^-$ is actually stronger than that of NO•, which is further discussed below.[56,57] As in the IR spectroelectrochemical measurements, this reduction is chemically fully reversible as shown in the inset of Figure 5. Finally, all attempts at chemical reduction (sodium anthracenide, KC_8) and isolation of **1-NO**$^-$ at room- and low-temperature were unsuccessful.

The spectroelectrochemical reductions of **2-NO**, **3-NO**, **4-NO** were also performed. The first half-wave reduction potentials of **2-NO** and **4-NO** are −1.18 V vs Fc/Fc$^+$, and $E_{1/2}$ for the first reduction of **3-NO** is slightly more positive at −1.13 V vs Fc/Fc$^+$ (Table 3). The UV−visible spectral changes upon reduction of **2-NO** are quite similar to those of **1-NO**, see Supporting Information, Figure S12. A decrease is observed in the band at 472 nm as two bands in the Q-region, at 519 and 548 nm, increase in absorbance. The reduction is chemically completely reversible. The formation of **2-NO**$^-$ is also completely reversible in IR experiments in 1,2-DCE-d_4 as shown in Figure 6 and Supporting Information, Figures S13−

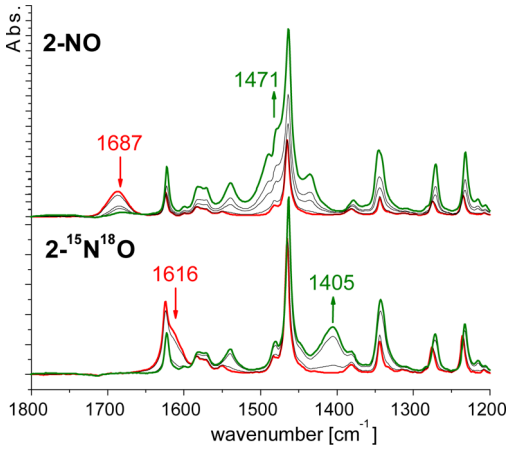

Figure 6. Infrared spectra for the spectroelectrochemical reduction of [Fe(T*o*-F_2PP)(NO)] (top, **2-NO**) and [Fe(T*o*-F_2PP)($^{15}N^{18}O$)] (bottom, **2-**^{15}**N**^{18}**O**). Difference spectra are provided in Figure 8.

S15. Using spectroelectrochemical IR measurements, a new ν(N−O) band corresponding to **2-NO**$^-$ is observed at 1471 cm^{-1}, which shifts to 1405 cm^{-1} upon $^{15}N^{18}O$ isotope labeling. Similar experiments were also performed for **3-NO** and **4-NO**, and the corresponding ν(N−O) values for these species and corresponding one-electron reduced complexes are provided in Table 2. For **3-NO**$^-$ a ν(N−O) band of ∼1500 cm^{-1} was observed (Supporting Information, Figure S16) and for **4-NO**$^-$ a N−O stretching frequency of 1482 cm^{-1} was identified (Supporting Information, Figure S17). The N−O stretching frequencies for **1-NO**$^-$ to **4-NO**$^-$ are in agreement with previous literature values as listed Table 2 and further illustrated in Figure 7. Importantly, *the N−O stretching*

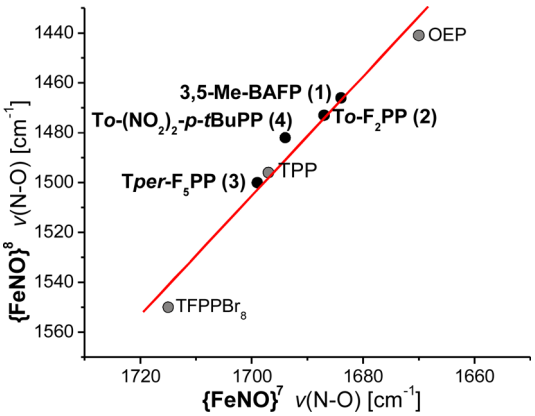

Figure 7. Comparison of N−O stretching frequencies in {FeNO}^{7} and {FeNO}^{8} porphyrin complexes.

frequencies of the {FeNO}^{8} complexes show a surprisingly strong, direct correlation with the ν(N−O) frequencies in the corresponding {FeNO}^{7} precursors. This indicates strongly correlated electronic structures in corresponding {FeNO}^{7} and {FeNO}^{8} pairs, and this is discussed in detail in Section 3.4.

3.3. The *trans* Effect of NO$^-$ in Low-Spin {FeNO}^{8} Complexes. Kadish and Ryan studied previously the reduction

dx.doi.org/10.1021/ic400977h | *Inorg. Chem.* XXXX, XXX, XXX−XXX

of {FeNO}^{7} complexes in the presence of pyridine (py) or other N-donor ligands.[19] In particular, it was shown by Choi and Ryan that the py binding constant to [Fe(TPP)(NO)] of 0.7 M^{-1} drops to ≤0.03 M^{-1} in [Fe(TPP)(NO)]$^-$,[56] providing a first indication that the NO^- ligand actually has a stronger *trans* effect than NO. In our investigations, we used 1-methylimidazole (MI) as a model for His in proteins. The corresponding binding constants of MI for our {FeNO}^{7} complexes, determined as described in the Experimental Section, are listed in Table 4. These results show that the largest K_{eq} for MI binding is found for **2-NO**, 2055 M^{-1},[58] which is therefore most favorable to (potentially) observe MI binding to an {FeNO}^{8} complex. With the addition of 50 equiv of MI, the N−O stretching frequency for the six-coordinate {FeNO}^{7} complex, **2$_{MI}$-NO**, is observed at 1636 cm^{-1}. This feature decreases upon one-electron reduction and a new band at 1473 cm^{-1} appears, corresponding to the {FeNO}^{8} complex. This is the same ν(N−O) as observed for **2-NO**$^-$, suggesting a loss of MI upon formation of the reduced product. As shown in Figure 8, the spectra obtained by reduction of **2-NO** and **2$_{MI}$-NO** are identical, demonstrating formation of five-coordinate **2-NO**$^-$ in both cases. According to BP86/TZVP calculated N−O stretching frequencies of five-coordinate [Fe(P)(NO)]$^-$ and six-coordinate [Fe(P)(MI)(NO)]$^-$, binding of MI to [Fe(P)(NO)]$^-$ should shift ν(N−O) to lower energy by at least 15 cm^{-1} as shown in Table 5. $^{15}N^{18}O$ isotope labeling further confirms these findings: the observed stretching frequency upon reduction of [Fe(T*o*-F_2PP)(MI)($^{15}N^{18}O$)] at 1405 cm^{-1} is exactly identical to **2-$^{15}N^{18}O$**$^-$. The reduction is chemically completely reversible (see Supporting Information, Figures S21 and S22) and after reoxidation the starting six-coordinate complexes, **2$_{MI}$-NO** and **2$_{MI}$-$^{15}N^{18}O$** are regenerated.

Table 4. Equilibrium Constants, K_{eq} [M^{-1}], and Free Reaction Energies, ΔG [kcal/mol], for the Reaction of [Fe(TPP*)(NO)] + MI ⇄ [Fe(TPP*)(MI)(NO)]

complex	K_{eq}	ΔG	ref
[Fe(TPP)(NO)]	26	−1.9	58
[Fe(3,5-Me-BAFP)(NO)] (**1-NO**)	76	−2.6	*t.w.*
[Fe(T*o*-$(NO_2)_2$-*p*-tBuPP)(NO)] (**4-NO**)	714	−3.9	*t.w.*
[Fe(To-F_2PP)(NO)] (**2-NO**)	2055	−4.5	58
[Fe(To-F_2PP)(NO)]$^-$ (**2-NO**$^-$)	≪ 0.2	≫ +1	*t.w.*

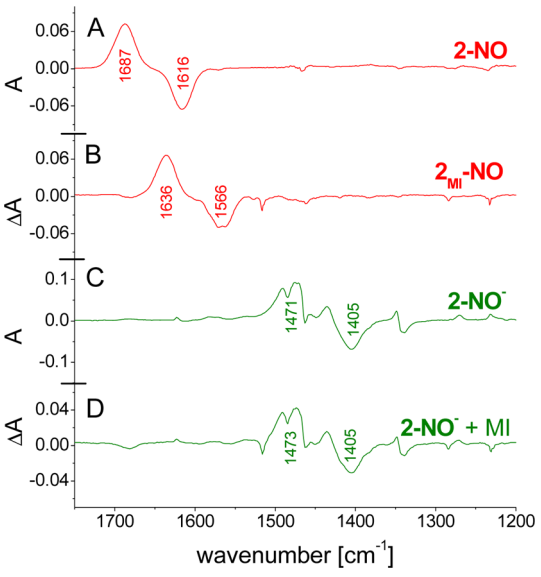

Figure 8. NO − $^{15}N^{18}O$ IR difference spectra for the spectroelectrochemical reduction of [Fe(T*o*-F_2PP)(NO)] in the absence (A: {FeNO}^{7}, C: {FeNO}^{8}) and presence (B: {FeNO}^{7}, D: {FeNO}^{8}) of MI.

Increasing the amount of MI to 170 equiv still shows formation of N−O stretching frequencies at 1473 and 1405 cm^{-1} for the natural abundance isotopes and $^{15}N^{18}O$ complexes, respectively. Using this, we can *estimate* the upper limit of the MI binding constant to **2-NO**$^-$ to be 0.2 M^{-1}. Using the Van't Hoff equation at 298.15 K this corresponds to an unfavorable Gibbs free energy, ΔG, of +1 kcal/mol for MI binding as listed in Table 4. This K_{eq} is calculated assuming 10% conversion to **2$_{MI}$-NO**$^-$ at 170 equiv of MI—which is likely an overestimate. As a result, the actual K_{eq} for MI binding to **2-NO** is, in reality, significantly lower than 0.2 M^{-1}. DFT geometry optimizations and calculated N−O stretching frequencies of [Fe(P)(MI)(NO)] and [Fe(P)(MI)(NO)]$^-$ support the strengthened thermodynamic *σ-trans* effect of NO^- in {FeNO}^{8} porphyrin complexes compared to NO in the {FeNO}^{7} analogues. The BP86/TZVP calculated Fe−N_{MI} bond length in [Fe(P)(MI(NO)]$^-$ is 2.45 Å (see Figure 9), close to nonbonding compared to 2.18 Å for [Fe(P)(MI)-(NO)] (see Table 5). Hence, NO^- has in fact the strongest *trans* effect when compared to NO, CO, O_2, and other diatomics in ferrous heme complexes!

3.4. Electronic Structure of {FeNO}^{8} Porphyrin Complexes in Comparison to the Analogous {FeNO}^{7} Species. The new spectroscopic data reported in this study for the complexes **1-NO**$^-$ to **4-NO**$^-$ significantly broaden our knowledge base of corresponding {FeNO}^{8} heme complexes (see Table 2) and, for the first time, allow for a detailed correlation of the electronic structures of analogous {FeNO}^{7} and {FeNO}^{8} species. As shown in Figure 7, there is a surprisingly strong correlation between the N−O stretching frequencies of analogous {FeNO}^{7} and {FeNO}^{8} complexes. This implies that the nature of the singly occupied molecular orbital (SOMO) that is occupied with a second electron upon reduction of the complexes from {FeNO}^{7} to {FeNO}^{8} does **not** change to a significant degree in this process; that is, whatever the composition of this MO is in the {FeNO}^{7} complex is *preserved* in the {FeNO}^{8} case. This further implies that the properties of the {FeNO}^{8} complexes investigated here in detail actually provide insight into the nature of the SOMO in the {FeNO}^{7} precursors, and in this way, into the electronic structures of both the {FeNO}^{7} and {FeNO}^{8} complexes.

Based on previous work,[57] detailed descriptions of the electronic structures of five- and six-coordinate ferrous heme-nitrosyls, {FeNO}^{7}, have been obtained. In these complexes, iron is in the +2 oxidation state and low-spin, leading to a $[t_2]^6[e]^0$ electron configuration of the metal. NO is a radical with one unpaired electron, which causes the resulting Fe(II)-NO adduct to have a total spin of S = 1/2. Hence, from a theoretical point of view, the spin-unrestricted scheme has to be applied to analyze bonding in the {FeNO}^{7} complexes, which distinguishes between majority (α) and minority (β) spin MOs. In the five-coordinate case, strong donation from the singly occupied π^* orbital of NO that is located in the Fe−N−O plane (α−π^*_h (h = horizontal) in the spin-unrestricted formalism) into the empty d_{z^2} orbital of iron is observed, leading to the formation of a strong Fe-NO σ bond. The SOMO that results from this interaction is the bonding

dx.doi.org/10.1021/ic400977h | *Inorg. Chem.* XXXX, XXX, XXX−XXX

Table 5. BP86/TZVP Calculated Geometric and Vibrational Parameters of Five- and Six-Coordinate {FeNO}^{7} and {FeNO}^{8} Heme Complexes (P^{2-} = porphine dianion)

	geometric parameters [Å] [deg]					vibrational frequencies [cm^{-1}]	
complex	ΔFe−N_{NO}	ΔN−O	ΔFe−N_{MI}	ΔFe−N_{porph}	∠Fe−N−O	ν(Fe−NO)	ν(N−O)
five-coordinate							
[Fe(P)(NO)]	1.704	1.179		2.019	146	595	1703
$[Fe(P)(NO)]^-$	1.786	1.206		2.011	125	568/(428)	1533
six-coordinate							
[Fe(P)(MI)(NO)]	1.734	1.186	2.179	2.021	140	609	1662
$[Fe(P)(MI)(NO)]^-$	1.805	1.210	2.451	2.015	124	543/(434)	1518

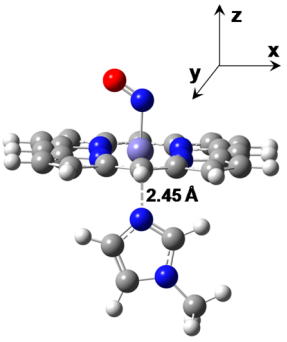

Figure 9. Model system $[Fe(P)(MI)(NO)]^-$, where P = $porphine^{2-}$ and MI = 1-methylimidazole, and applied coordinate system. The structure shown is calculated with BP86/TZVP.

Scheme 1. Molecular Orbitals Proposed to Be Responsible for the *σ-trans* Effect of NO in Six-Coordinate Ferrous Heme Complexes

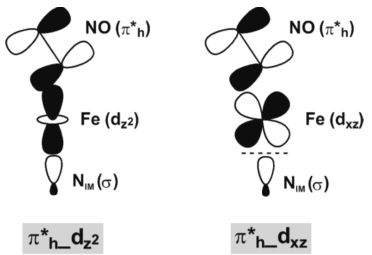

combination of $\alpha-\pi^*_h$ and α-d_{z^2}, labeled $\pi^*_h\_d_{z^2}$ in Scheme 1, left. Based on experimentally calibrated DFT (B3LYP) calculations,[58,59] this leads to a complete delocalization of the unpaired electron of NO, with resulting spin densities of about 50% on Fe and 50% on NO.[60] In addition, strong π-backbonding is observed between the unoccupied π^*_v orbital of NO (v = vertical, orthogonal the Fe−N−O plane) and the d_{yz} orbital of iron (in the applied coordinate system where the *z* axis is aligned with the heme-normal, and the Fe−N−O unit is in the *xz* plane). For a more detailed analysis see ref 57, 60. Additional contributions to the backbond are observed between the unoccupied $\beta-\pi^*_h$ orbital of NO and β-d_{xz} of iron. Upon coordination of an N-donor ligand (imidazole or His) in trans position to NO, a distinct weakening of the Fe-NO σ bond is observed. This induces a distinct drop in the Fe-NO force constant and corresponding Fe-NO stretching frequency in the six-coordinate case as observed experimentally.[58,61] In addition, the underlying *σ-trans* interaction between NO and imidazole leads to weak binding of imidazole in trans position to NO (K_{eq} is usually <50 M^{-1}).[57] This mechanism, the strong (thermodynamic) *σ-trans* effect of NO in low-spin {FeNO}^{7} complexes, is responsible for the activation of the NO sensor soluble guanylate cyclase.[62,63]

Although basic agreement has been achieved in the literature on the overall electronic structure description of ferrous heme-nitrosyls as described above, the specific details are still controversial. The reason for this is that DFT methods are generally not very accurate in describing the properties of the Fe−N−O unit in these complexes.[57,62,64] In particular, the spin density distribution, that is, the distribution of the unpaired electron of NO over the Fe-NO unit, is strongly affected by the chosen DFT method,[65] as documented nicely by Pierloot and co-workers.[66,67] Whereas gradient-corrected functionals generally lead to metal-based spin (>60% spin density on iron), hybrid functionals give a more unified distribution of the spin density over the whole Fe−N−O unit.[57,67] It is therefore most important to compare calculated properties to experiment to better assess the quality of the calculated results, in particular spectroscopic properties are a good way to gauge the quality of quantum-chemical calculations. In principle, EPR *g* values and hyperfine coupling constants (especially those of the coordinated ^{14}N atom of NO) should be a good experimental probe for the spin density distribution in ferrous heme-nitrosyls. In this case, it has been shown that gradient-corrected functionals[59,68,69]perform slightly better than hybrid functionals[59] for the calculation of *g* tensors and hyperfine coupling constants. These types of calculations, however, generally show quite large deviations from experiment and are also strongly dependent on the geometry and the applied basis set.[70] Thus, it is difficult to judge the quality of the overall description solely based on comparisons of EPR parameters.[65] On the other hand, calculated Fe-NO vibrational frequencies and force constants, which directly reflect the strength of the Fe-NO bond, show very clear trends when comparing the results from calculations using gradient-corrected and hybrid functionals. Here, gradient-corrected functionals tend to overemphasize electron delocalization and, as demonstrated now for many cases,[57] lead to an overestimation of metal−ligand covalencies, and hence, bond strengths. This is reflected by the calculated Fe-NO stretching frequencies in five- and six-coordinate ferrous heme-nitrosyls, predicted at about 600 cm^{-1}, whereas experimentally, these are observed at 515−530 and ∼440 cm^{-1}, respectively (see Table 2). In contrast, B3LYP predicts the Fe-NO stretch at 540−580 and ∼420 cm^{-1} for the five- and six-coordinate {FeNO}^{7} complexes, respectively, which is in much better agreement with experiment (see also ref 57). The overestimate of the covalency of the Fe-NO bond with the gradient-corrected functionals goes along with a significant quenching of the spin density on the NO ligand.

Because of this, the spin density distributions calculated with hybrid functionals (see above) can overall be expected to be more reliable, and hence, these should be in closer agreement

dx.doi.org/10.1021/ic400977h | *Inorg. Chem.* XXXX, XXX, XXX−XXX

with the electronic structures of the real complexes. Calculated Fe-NO binding energies further support these conclusions. Hybrid functionals are in fact able to predict quite accurate Fe-NO binding energies when the important van-der-Waals interactions are included.[71] In contrast, gradient-corrected functionals greatly overestimate NO binding energies,[71] in agreement with the overestimation of the Fe-NO bond strengths in these cases.

Importantly, the experimental properties of the analogous $\{FeNO\}^8$ complexes investigated here provide further key insight into the properties of the SOMO in $\{FeNO\}^7$ systems. Whereas previous DFT results characterize the SOMO of ferrous heme-nitrosyls as the *bonding* combination of $\alpha-\pi^*_h$ and α-d_{z^2}, $\pi^*_h\_d_{z^2}$, as described above (see Scheme 1, left),[58,72] it was recently proposed that for the corresponding six-coordinate complexes, this orbital should be considered the *antibonding* combination between $\alpha-\pi^*_h$ and α-d_{xz}, resulting in a SOMO that is strongly π-antibonding in nature as illustrated in Scheme 1, right.[73] This would de facto eliminate the Fe-NO σ bond in six-coordinate $\{FeNO\}^7$ complexes. However, there are several experimental observations that argue against this notion.[65] First, the strong thermodynamic σ-*trans* effect of NO requires the presence of a distinct σ bond; in comparison, the strongly π backbonding ligand CO does not mediate much of a *trans* effect.[62,74] Second, the results of this study demonstrate that adding an electron to the SOMO of six-coordinate $\{FeNO\}^7$ complexes leads to a further increase of the *trans* effect as discussed above, which is evident from a further, dramatic decrease of the MI binding constant in the $\{FeNO\}^8$ case. As inferred from the strong correlation of ν(N−O) discussed above (see Figure 7), DFT calculations further confirm that this is not due to a change in the nature of the SOMO, but simply caused by the addition of one electron to this MO. As shown in Figure 10 and Table 6, the charge

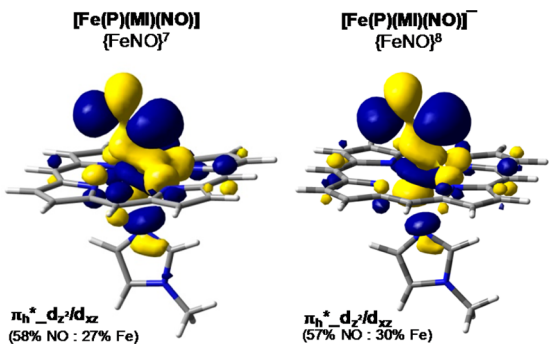

Figure 10. Key $\pi^*_h\_d_{z^2}/d_{xz}$ molecular orbitals of (left) [Fe(P)(MI)(NO)] and (right) $[Fe(P)(MI)(NO)]^-$ which defines the thermodynamic σ-*trans* effect in ferrous porphyrin systems. Calculated with B3LYP/TZVP on BP86/TZVP optimized structures.

Table 6. Charge Contributions of Key σ Bonding Orbitals[a] for $[Fe(P)(MI)(NO)]^{0/1-}$

			Fe	NO	N_{MI}
complex	orbital	label	d	s+p	s+p
[Fe(P)(MI)(NO)]	⟨120⟩	$\pi^*_h\_d_{z^2}/d_{xz}$	27	58	2
$[Fe(P)(MI)(NO)]^-$	⟨122⟩	$\pi^*_h\_d_{z^2}$	30	57	1

[a]Calculated with B3LTP/TZVP for BP86/TZVP optimized structures (P^{2-} = porphine dianion).

Scheme 2. Electronic Structure of Low-Spin $\{FeNO\}^7$ and $\{FeNO\}^8$ Complexes

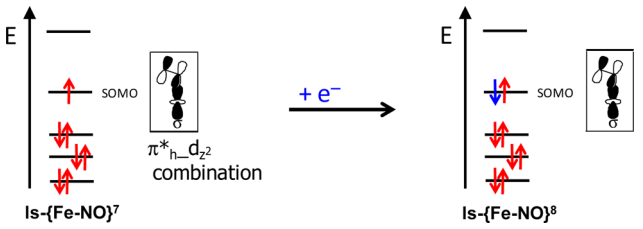

contributions of this MO are in fact invariant to the one-electron reduction. This is further illustrated in Scheme 2. Third, previous work by Ryan and co-workers on [Fe(TPP)(NO)] has shown that the Fe-NO stretching frequency *increases* in $\{FeNO\}^8$ compared to the analogous $\{FeNO\}^7$ complexes (see Table 2).[20] This is because the one-electron reduction leads to an increase in σ bonding by double occupation of the SOMO (accompanied by a reduction in π backbonding between $\beta-\pi^*_h$ and β-d_{xz}), causing a noticeable strengthening of the Fe-NO bond upon reduction. This finding disagrees with the idea that the SOMO is strongly π antibonding in nature; in this case, occupation of this MO should lead to a distinct weakening of the Fe-NO bond, and a significant drop in the Fe-NO stretching frequency, which is not observed experimentally. In conclusion, all these findings provide strong evidence that the SOMO of $\{FeNO\}^7$ complexes is predominantly σ-bonding in nature, whereas the admixture of $\pi^*_h\_d_{xz}$ character is small.

3.5. Reactivity of $\{FeNO\}^8$ Complexes. *Bulk Electrolysis in the Presence of Acid.* Initial attempts at protonation of Fe(II)-NO^- heme complexes were focused on bulk electrolysis of the corresponding $\{FeNO\}^7$ complexes (at mM concentrations) in the presence of several equivalents of acetic acid (see also ref 75). For example, reduction of **2-NO** in THF at room temperature at −0.9 V vs Ag wire resulted in a ferrous product by UV−visible and EPR spectroscopy. The product, however, does not show any isotope sensitive IR bands in the 1700−1200 cm^{-1} region as would be expected for a ferrous nitrosyl or nitroxyl product complex, and analysis of the reaction head space did not show the presence of any N_2O. Interestingly, coulometry indicated that the reaction continued to progress well past one equivalent of electrons. In fact, the current did not stabilize until ∼5 equiv of electrons were passed. This implies that the formed Fe(II)-NHO complex is further reduced under our electrolysis conditions. As proposed previously for heme systems,[76,77] we expect our reaction to proceed as follows

$$Fe(II)-NO(radical) + e^- \rightarrow Fe(II)-NO^- \quad (3)$$

$$Fe(II)-NO^- + H^+ \rightarrow Fe(II)-NHO \quad (4)$$

$$Fe(II)-NHO + 2e^- + 2H^+ \rightarrow Fe(II)-NH_2OH \quad (5)$$

$$Fe(II)-NH_2OH + 2e^- + 2H^+ \rightarrow Fe(II) + NH_3 + H_2O \quad (6)$$

where the reduction potentials of the intermittently formed Fe(II)-NHO and Fe(II)-NH_2OH complexes observed here are more positive than that of **2-NO** (in agreement with ref 75). Indeed, ammonia analysis using Russell's hypochlorite-phenol[25,26] method yielded ∼1 equiv of NH_3 in the product mixture. As such, we propose our product to be a ferrous heme

dx.doi.org/10.1021/ic400977h | Inorg. Chem. XXXX, XXX, XXX−XXX

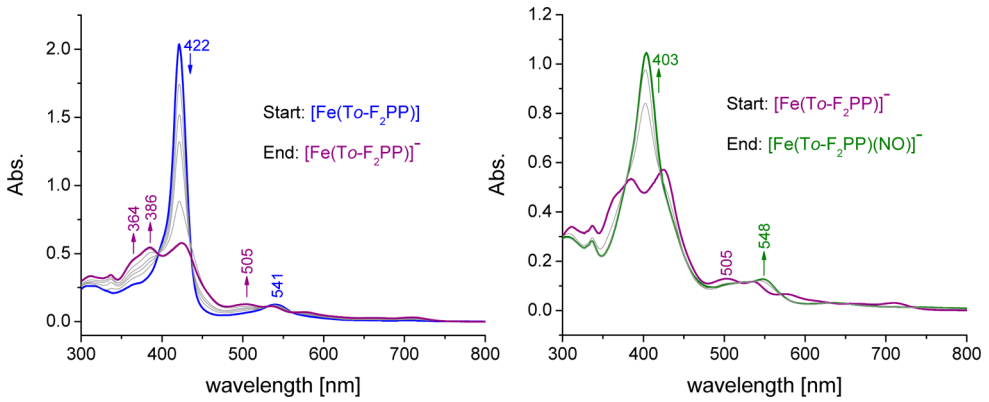

Figure 11. UV−vis spectra for the one-electron reduction of [Fe(T*o*-F_2PP)] (**2**, blue) to [Fe(T*o*-F_2PP)]$^-$ (**2**$^-$, purple), shown at left, and subsequent reaction with 100 μL of NO(g) (right, green) in THF at room temperature.

complex with bound ammonia or water. Similar reactivity was observed for the reduction of **1-NO** in the presence of acetic acid. Based on these observations, we speculate that ferrous hemes could act as catalysts for the electrochemical reduction of NO to NH_3 and water, similar to assimilatory nitrite reductases.[75] However, because of the unfavorable reduction potential of the first step (eq 3), these catalysts would not be very energy efficient. Furthermore, this procedure can therefore not be applied for the preparation of ferrous heme-HNO complexes.

As protonation of the formed {FeNO}^{8} complexes in the presence of an applied potential results in further reduction of the generated Fe(II)-HNO species, it is essential to separate the reduction of the {FeNO}^{7} complex from the protonation of the resulting {FeNO}^{8} species, see eqs 3 and 4 above. To accomplish this task, bulk electrolysis of **2-NO** was performed in the absence of acid to first convert all of the material into **2-NO**$^-$. This step could then be followed by addition of acid. However, the reduction of **2-NO** is unfortunately unreliable and often leads to significant decomposition of **2-NO**$^-$, so this process is also not feasible for practical applications.

Generation of {FeNO}^{8} Complexes via Iron(I) Intermediates. Because of these difficulties, we devised an alternate route based on the observation that ferrous hemes can be reversibly reduced by bulk electrolysis (eq 7).[78] The generated, formally iron(I), species (this actually corresponds to a reduction of the porphyrin ligand as discussed below) could then in principle be reacted with NO, resulting in the desired {FeNO}^{8} complex:

$$[\text{Fe(porphyrin)}] + e^- \rightarrow [\text{Fe(porphyrin)}]^- \quad (7)$$

$$[\text{Fe(porphyrin)}]^- + \text{NO} \rightarrow [\text{Fe(porphyrin)(NO)}]^- \quad (8)$$

Here, the porphyrin ligand stores the electron necessary for reduction of the Fe-NO unit. This approach has been applied to [Fe(T*o*-F_2PP)] (**2**) and the resulting in situ UV−visible spectra are provided in Figure 11. Upon one-electron reduction in THF, the sharp Soret band at 422 nm decreases in intensity while new broad features at 364 and 386 nm appear (Figure 11, left). This drastic decrease in intensity is characteristic of a loss in porphyrin conjugation indicating that the product complex is formally a Fe(II)-porphyrin$^{\bullet-}$ (porphyrin radical) species.[79]

Upon addition of 100 μL of NO gas to **2**$^-$, see Figure 11 (right), the desired **2-NO**$^-$ is generated. Interestingly, if only 10 μL of NO gas are added, a unique species with a Soret band at 416 nm is observed (Supporting Information, Figure S24). The nature of this species (likely a ferrous complex) requires further

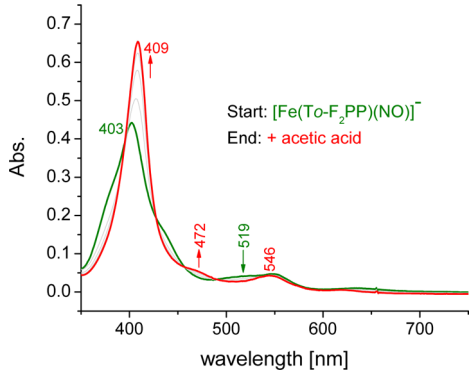

Figure 12. UV−visible spectra for the reaction of [Fe(T*o*-F_2PP)(NO)]$^-$ (**2-NO**$^-$, green) with 5 equiv of acetic acid in THF at room temperature. The resulting spectrum (red) is in agreement with formation of [Fe(T*o*-F_2PP)(NO)] (**2-NO**).

study, but may correspond to a hyponitrite type intermediate. **2-NO**$^-$ reacts further with free NO in solution to form **2-NO**, as evident from UV−visible spectroscopy. To combat this reaction, as soon as **2-NO**$^-$ is generated, the solution is sparged with inert gas to remove free NO from the reaction vessel. The further reaction of **2-NO**$^-$ with NO suggests that **2-NO**$^-$ actually reduces free NO, forming **2-NO** and NO$^-$, the latter then decomposes in an unknown fashion. In fact, the reduction potential of free NO is −0.8 V vs SHE,[80] more positive than the resting potential of **2-NO**$^-$. This result indicates that the reaction of NO with deprotonated Fe(II)-NO$^-$ complexes does not induce N−N bond formation, which therefore likely requires the presence of protons (see discussion in ref 17). Therefore, the protonation of **2-NO**$^-$ was explored next.

Generation of the First Ferrous Heme-HNO Model Complex. Addition of acetic acid to **2-NO**$^-$ in THF resulted in the formation of **2-NO**, as shown in Figure 12. EPR spectroscopy of the reaction mixture shows the characteristic $S = 1/2$ signal, indicative of a low-spin ferrous heme-nitrosyl complex (data not shown). This is similar to the reactivity of [Fe(TPP)(NO)]$^-$ and [Fe(TFPPBr$_8$)(NO)]$^-$ with acid where the corresponding {FeNO}^{7} complex and 0.5 equiv of H_2 are reported as products[20,22]

$$2[\text{Fe(porphyrin)(NHO)}] \rightarrow 2[\text{Fe(porphyrin)(NO)}] + H_2 \quad (9)$$

dx.doi.org/10.1021/ic400977h | *Inorg. Chem.* XXXX, XXX, XXX−XXX

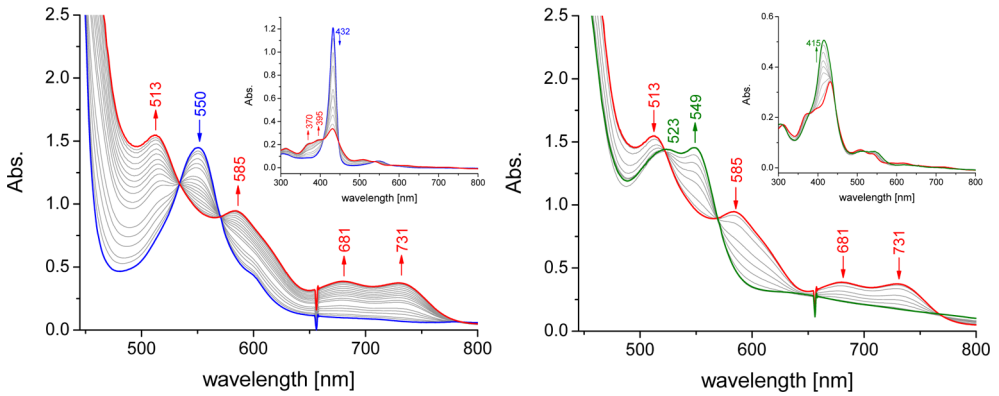

Figure 13. UV−vis spectra for the one-electron reduction of [Fe(3,5-Me-BAFP)] (0.2 mM **1**, blue) to [Fe(3,5-Me-BAFP)]$^-$ (**1**$^-$, red), shown at left, and subsequent reaction with 100 μL of NO (g) in THF at room temperature resulting in formation of [Fe(3,5-Me-BAFP)(NO)]$^-$ (**1-NO**$^-$, right, green). Inset: same reactions at ∼0.02 mM heme concentrations.

This result is perhaps not surprising as To-F_2PP^{2-}, similar to TPP^{2-} and TFPPBr$_8^{2-}$, lacks the steric protection needed to prevent this disproportionation of the Fe-NHO unit. In this sense, the reaction of the bis-picket fence porphyrin complex [Fe(3,5-Me-BAFP)(NO)]$^-$ (**1-NO**$^-$) with acid is of extreme interest.

To this end, bulk electrolysis of [Fe(3,5-Me-BAFP)] (**1**) in THF was performed at room temperature. The in situ UV−visible spectra for the one-electron reduction to **1**$^-$ are reported in Figure 13 (left). EPR spectroscopy (Supporting Information, Figure S25) shows a sharp isotropic spectrum with a g-value of 1.99 for **1**$^-$ indicating porphyrin ring reduction to an S = 1/2 complex. Addition of 100 μL of NO to **1**$^-$ at room temperature results in formation of **1-NO**$^-$ with a Soret band at 415 nm (consistent with spectroelectrochemical measurements), as shown in Figure 13 (right). Subsequent reaction of **1-NO**$^-$ with ∼1.4 equiv of acetic acid indicates formation of a new complex, [Fe(3,5-Me-BAFP)(NHO)] (**1-NHO**), with the Soret band at 426 nm and the Q-band observed at 545 nm, see Figure 14. Excitingly, this species does not correspond to **1-NO**, which instead shows a Soret band of 422 nm in THF. In addition, gas IR analysis of the reaction headspace after addition of acid indicates no formation of N_2O (Supporting Information, Figure S26), which proves that the complex does not simply lose HNO after protonation. This is in contrast to the protonation of **2-NO**$^-$, discussed above, which instantly undergoes decomposition to **2-NO**. To further confirm the identity of the heme HNO complex, 2 equiv of phosphazene base (P_1-*t*Bu-tris(tetramethylene)) was reacted with the presumable formed **1-NHO**. Upon addition of base, see Figure 15, UV−visible spectroscopy shows essentially complete

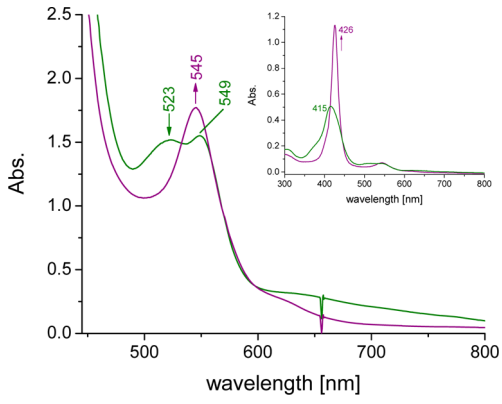

Figure 14. UV−visible spectra for the reaction of [Fe(3,5-Me-BAFP)(NO)]$^-$ (0.2 mM **1-NO**$^-$, green) with 5 equiv of acetic acid in THF at room temperature. The resulting spectrum is shown in purple. Inset: same reaction at ∼0.02 mM heme concentration.

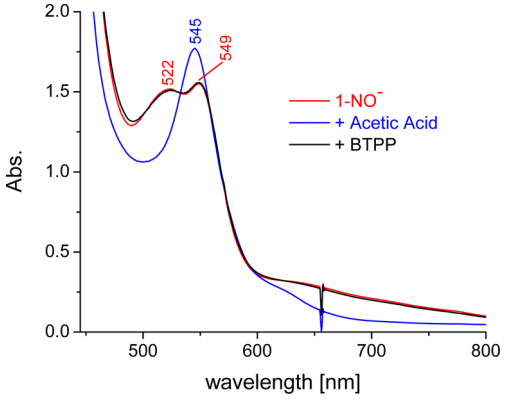

Figure 15. UV−visible spectrum for the reaction of 0.2 mM [Fe(3,5-Me-BAFP)(NO)]$^-$ (**1-NO**$^-$, red) with 1.4 equiv of acetic acid (blue) to generate **1-NHO** followed by deprotonation of **1-NHO** with 2 equiv of phosphazene base, P_1-*t*Bu-tris(tetramethylene) (BTPP, black) to regenerate **1-NO**$^-$.

reformation of **1-NO**$^-$. Further addition of acetic acid then results in ∼quantitative reformation of **1-NHO**. Finally, the UV−vis spectral properties of **1-NHO** are similar to Farmer's Mb(II)-NHO complex.[23] Both compounds show typical ferrous porphyrin absorption spectra with Soret band positions at 423 (Mb-NHO complex) and 426 nm (**1-NHO**), further supporting the idea that **1-NHO** in fact contains a bound HNO ligand.

The formed **1-NHO** complex is EPR silent and decays at a slow rate to **1-NO** as evidenced by EPR, see Supporting Information, Figure S27, and UV−visible spectroscopy. Spin quantification of the EPR spectra (Supporting Information, Figure S28) indicate that after 2 h (0.2 mM, room temperature) 27% of the formed **1-NHO** is decomposed to **1-NO** and after 20 h the decomposition is essentially complete (90% of **1-NO** are detected). This is consistent with UV−visible spectroscopy. Thus, for the first time, we are able to delay the disproportionation of bound HNO through the use of a bis-picket fence porphyrin to generate the first stable ferrous heme-

dx.doi.org/10.1021/ic400977h | *Inorg. Chem.* XXXX, XXX, XXX−XXX

HNO model complex reported to this date. With this complex in hand, detailed reactivity studies on a heme-bound HNO complex can be performed in the future. Here, we explored whether a ferrous heme-HNO complex is reactive toward NO, as proposed recently in a DFT study on the mechanism of P450nor.[14] Surprisingly, addition of low equivalents of NO to **1-NHO** at room temperature resulted in immediate formation of **1-NO** as evident from UV−vis spectroscopy, where HNO is presumably displaced by the stronger ligand NO. No N−N bond formation results from the reaction of **1-HNO** with NO, indicative that ferrous heme-HNO complexes are **not** competent intermediates in NO reductases. To further solidify this conclusion, analogous investigations on six-coordinate HNO complexes with an axial MI ligand are necessary, which are currently in progress. The biological implications of these results are discussed in the next section.

4. CONCLUSIONS

In this work, the new bis-picket fence porphyrin ferrous-nitrosyl complex [Fe(3,5-Me-BAFP)(NO)] has been prepared and crystallographically characterized, showing a unique conformation of the Fe-NO unit. This complex, along with three ferrous heme-nitrosyls with electron-poor porphyrins, is then used to generate a series of four new ferrous heme-nitroxyl, {FeNO}^{8}, complexes. The N−O stretching frequency of the resulting, reduced complex [Fe(3,5-Me-BAFP)(NO)]$^-$ is observed at 1466 cm^{-1}. With the electron-poor hemes, the nitroxyl complexes show higher values for ν(N−O) in the 1470−1500 cm^{-1} range. With these new nitroxyl complexes in hand, the number of well-characterized heme {FeNO}^{8} complexes is now increased to seven, which, for the first time, allows for the systematic analysis of trends in the properties of these species (see Table 2). Importantly, a very strong correlation of ν(N−O) between the {FeNO}^{7} precursors and the resulting {FeNO}^{8} species is observed, which indicates that the nature of the SOMO that becomes double occupied when the {FeNO}^{7} complex is reduced (see Scheme 2) does not change in the {FeNO}^{8} species. In other words, whatever the nature of this MO is in the {FeNO}^{7} complex is preserved in the {FeNO}^{8} species, and this result is further supported by DFT calculations. We further investigated whether a six-coordinate {FeNO}^{8} complex can be generated using the six-coordinate precursor [Fe(T*o*-F$_2$PP)(MI)(NO)], which has a very high affinity for MI.[58] However, upon one-electron reduction, this complex forms the five-coordinate species [Fe(T*o*-F$_2$PP)(NO)]$^-$. We estimate the binding constant, K_{eq}, for MI binding to [Fe(T*o*-F$_2$PP)(NO)]$^-$ to be $\ll$0.2 M^{-1}, at least 4 orders of magnitude smaller than that of MI binding to [Fe(T*o*-F$_2$PP)(NO)], in good agreement with previous results for py binding to [Fe(TPP)(NO)]$^-$.[56] These results demonstrate that NO$^-$ has the strongest *trans* effect when compared to NO, CO, and O$_2$ in ferrous heme systems. The increase of the *trans* effect upon one-electron reduction of the {FeNO}^{7} complex, in combination with the strong correlation of the electronic structures of analogous {FeNO}^{7} and {FeNO}^{8} complexes mentioned above, provides further direct experimental proof that the SOMO in ferrous heme-nitrosyls is in fact Fe-NO σ-bonding in nature. This finding, although quite established in the literature, has recently been challenged.[73]

The studies into the spectroscopic properties and electronic structures of ferrous heme-nitroxyl complexes mentioned above are all based on spectroelectrochemical measurements. However, to prepare a ferrous heme-HNO complex and to perform reactivity studies, a preparation of bulk material of the reduced complexes is necessary, which has been generally found difficult. We were able to achieve this via a completely new synthetic approach that starts from the four-coordinate ferrous precursor, [Fe(porphyrin)], which can be bulk-reduced by one electron to yield the stable (under rigorous exclusion of O$_2$), formally iron(I) complex [Fe(porphyrin)]$^-$. Importantly, this species can then be reacted with NO to generate bulk material of pure {FeNO}^{8} complexes as shown in this work. The reactivity of the resulting nitroxyl complexes was then tested. First, the complex [Fe(T*o*-F$_2$PP)(NO)]$^-$ reacts with acetic acid to generate the corresponding {FeNO}^{7} complex and 0.5 equiv of H$_2$, as previously reported for similar species, because of disproportionation of an intermittently formed HNO complex. However, the corresponding sterically hindered 3,5-Me-BAFP^{2-} complex shows unique reactivity, effectively blocking the disproportionation of bound HNO and *generating the first ferrous heme-HNO model complex*, [Fe(3,5-Me-BAFP)(NHO)]. This HNO complex is stable in solution at room temperature for several hours and can be further deprotonated with phosphazene base to regenerate the corresponding [Fe(3,5-Me-BAFP)(NO)]$^-$ species. Hence, the bis-picket fence porphyrin provides a unique stabilization for the heme-bound HNO that has not been observed with any other porphyrin.

Finally, the reactivity of {FeN(H)O}^{8} complexes toward NO was tested. First, reaction of [Fe(T*o*-F$_2$PP)(NO)]$^-$ with NO results in reduction of free NO to NO$^-$ and oxidation of the ferrous nitroxyl complex to [Fe(T*o*-F$_2$PP)(NO)], and a similar process is seen for [Fe(3,5-Me-BAFP)(NO)]$^-$. Second, reaction of [Fe(3,5-Me-BAFP)(NHO)] with NO leads to displacement of the HNO ligand by NO, generating [Fe(3,5-Me-BAFP)(NO)], but no direct N−N bond formation is observed, which would generate a ferric heme-hyponitrite complex. These results have important biological implications. The lack of reactivity of the heme-HNO complex with NO with respect to N−N bond formation indicates that a ferrous heme-HNO complex is likely not catalytically competent for N−N bond formation and N$_2$O generation in Cyt. P450nor. This provides strong evidence, as proposed originally,[13,14] that a second protonation of the HNO complex is required to achieve hyponitrite formation. With respect to NorBC, recent computational studies have indicated that {FeNO}^{8} and in particular, {FeNHO}^{8} species should react with NO to induce N−N bond formation and hyponitrite generation,[17] but experimentally, we do not observe this reaction for either one of these complexes, casting doubt on the mechanistic proposal of a *cis*-heme b_3 mechanism[81,82] for this enzyme.

Future studies will focus on the characterization and isolation of [Fe(3,5-Me-BAFP)(NHO)] (**1-NHO**) and the generation of a corresponding six-coordinate complex with bound MI. The latter species can then be used to explore whether the presence of the axial ligand could influence the reactivity of the HNO complex with NO. Please note in this regard that the isolation of nitroxyl complexes after bulk electrolysis is difficult because of the large amounts of electrolyte present in solution, which also interferes with all attempts to crystallize **1-NHO**. New procedures are currently being developed to achieve this without decomposition of the complex. This work is in progress.

dx.doi.org/10.1021/ic400977h | *Inorg. Chem.* XXXX, XXX, XXX−XXX

■ ASSOCIATED CONTENT

Supporting Information

Further spectroscopic characterization (EPR, IR) of **1-NO**−**4-NO**, spectroelectrochemical data for the reduction of **1**, **1-NO**−**4-NO** and $\mathbf{2_{MI}}$**-NO** and the corresponding $^{15}N^{18}O$-labeled complexes, UV−vis titration of **1-NO** and **4-NO** with MI, spectroscopic data for the generation and slow decomposition of **1-NHO**, ^1H NMR data for the synthesis of H_2[(3,5-Me-BAFP)], and the complete ref 40. This material is available free of charge via the Internet at http://pubs.acs.org.

■ AUTHOR INFORMATION

Corresponding Author

*E-mail: lehnertn@umich.edu.

Notes

The authors declare no competing financial interest.

■ ACKNOWLEDGMENTS

This work was supported by the National Science Foundation (CHE-0846235 to N.L.). We acknowledge Dr. Jeff Kampf (University of Michigan) for his X-ray crystallographic analysis of [Fe(3,5-Me-BAFP)(NO)] (**1-NO**), and funding from NSF Grant CHE-0840456 for X-ray instrumentation. We particularly thank Dr. Michael D. Ryan (Marquette University) for helpful discussions on spectroelectrochemical techniques, and Ms. Ashley McQuarters for determining the extinction coefficients of [Fe(3,5-Me-BAFP)(NO)] and [Fe(3,5-Me-BAFP)].

■ REFERENCES

(1) Burney, S.; Tamir, S.; Gal, A.; Tannenbaum, S. R. *Nitric Oxide* **1997**, *1*, 130.
(2) Moncada, S.; Palmer, R. M.; Higgs, E. A. *Pharmacol. Rev.* **1991**, *43*, 109.
(3) Snyder, S. H. *Science* **1992**, *257*, 494.
(4) Bredt, D. S.; Snyder, S. H. *Annu. Rev. Biochem.* **1994**, *63*, 175.
(5) Ignarro, L. *Nitric Oxide: Biology and Pathobiology*; Academic Press: San Diego, CA, 2000.
(6) Nakahara, K.; Tanimoto, T.; Hatano, K.; Usuda, K.; Shoun, H. *J. Biol. Chem.* **1993**, *268*, 8350.
(7) Dabier, A.; Shoun, H.; Ullrich, V. *J. Inorg. Biochem.* **2005**, *99*, 185.
(8) Park, S.-Y.; Shimizu, H.; Adachi, S.; Nagagawa, A.; Tanaka, I.; Nakahara, K.; Shoun, H.; Obayashi, E.; Nakamura, H.; Iizuka, T.; Shiro, Y. *Nat. Struct. Biol.* **1997**, *4*, 827.
(9) Shimizu, H.; Park, S.-Y.; Lee, D. S.; Shoun, H.; Shiro, Y. *J. Inorg. Biochem.* **2000**, *81*, 191.
(10) Shiro, Y.; Fujii, M.; Iisuka, T.; Adachi, S.; Tsukamoto, K.; Nakahara, K.; Shoun, H. *J. Biol. Chem.* **1995**, *270*, 1617.
(11) Enemark, J. H.; Feltham, R. D. *Coord. Chem. Rev.* **1974**, *13*, 339.
(12) Obayashi, E.; Takahashi, S.; Shiro, Y. *J. Am. Chem. Soc.* **1998**, *120*, 12964.
(13) Lehnert, N.; Praneeth, V. K. K.; Paulat, F. *J. Comput. Chem.* **2006**, *27*, 1338.
(14) Riplinger, C.; Neese, F. *ChemPhysChem.* **2011**, *12*, 3192.
(15) Hino, T.; Matsumoto, Y.; Nagano, S.; Sugimoto, Y.; Fukumori, Y.; Murata, T.; Iwata, S.; Shiro, Y. *Science* **2010**, *330*, 1666.
(16) Lehnert, N.; Berto, T. C.; Galinato, M. G. I.; Goodrich, L. E. The Role of Heme-Nitrosyls in the Biosynthesis, Transport, Sensing, and Detoxification of Nitric Oxide (NO) in Biological Systems: Enzymes and Model Complexes. In *Handbook of Porphyrin Science*; Kadish, K. M., Smith, K., Guilard, R., Eds.; World Scientific: Singapore, 2012; Vol. *14*, p 1.
(17) Yi, J.; Morrow, B. H.; Campbell, A. L. O. C.; Shen, J. K.; Richter-Addo, G. B. *Chem. Commun.* **2012**, *48*, 9041.
(18) Lancon, D.; Kadish, K. M. *J. Am. Chem. Soc.* **1983**, *105*, 5610.
(19) Olson, L. W.; Schaeper, D.; Lancon, D.; Kadish, K. M. *J. Am. Chem. Soc.* **1982**, *104*, 2042.
(20) Choi, I. K.; Liu, Y.; Feng, D. W.; Paeng, K. J.; Ryan, M. D. *Inorg. Chem.* **1991**, *30*, 1832.
(21) Wei, Z.; Ryan, M. D. *Inorg. Chem.* **2010**, *49*, 6948.
(22) Pellegrino, J.; Bari, S. E.; Bikiel, D. E.; Doctorovich, F. *J. Am. Chem. Soc.* **2010**, *132*, 989.
(23) Sulc, F.; Immoos, C. E.; Pervitsky, D.; Farmer, P. J. *J. Am. Chem. Soc.* **2004**, *126*, 1096.
(24) Kumar, M. R.; Pervitsky, D.; Chen, L.; Poulos, T.; Kundu, S.; Hargrove, M. S.; Rivera, E. J.; Diaz, A.; Colon, J. L.; Farmer, P. J. *Biochemistry* **2009**, *48*, 5018.
(25) Choi, I. K.; Wei, Z.; Ryan, M. D. *Inorg. Chem.* **1997**, *36*, 3113.
(26) Russell, J. A. *J. Biol. Chem.* **1944**, *156*, 457.
(27) Quast, H.; Dietz, T.; Witzel, A. *Liebigs Ann.* **1995**, 1495.
(28) Ghiladi, R. A.; Kretzer, R. M.; Guzei, I.; Rheingold, A. L.; Neuhold, Y.-M.; Hatwell, K. R.; Zuberbuhler, A. D.; Karlin, K. D. *Inorg. Chem.* **2001**, *40*, 5754.
(29) Peters, M. V.; Stoll, R. S.; Goddard, R.; Buth, G.; Hecht, S. *J. Org. Chem.* **2006**, *71*, 7840.
(30) Rose, E.; Kossanyi, A.; Quelquejeu, M.; Soleilhavoup, M.; Duwavran, F.; Bernard, N.; Lecas, A. *J. Am. Chem. Soc.* **1996**, *118*, 1567.
(31) Lulinski, S.; Servatowski, J. *J. Org. Chem.* **2003**, *68*, 5384.
(32) Tohara, A.; Sugawara, Y.; Sato, M. *J. Porphyrins Phthalocyanines* **2006**, *10*, 104.
(33) Adler, A. D.; Longo, F. R.; Kampas, F.; Kim, J. *J. Inorg. Nucl. Chem.* **1970**, *32*, 2443.
(34) Scheidt, W. R.; Frisse, M. E. *J. Am. Chem. Soc.* **1975**, *97*, 17.
(35) Berto, T. C.; Hoffman, M. B.; Murata, Y.; Landenberger, K. B.; Alp, E. E.; Zhao, J.; Lehnert, N. *J. Am. Chem. Soc.* **2011**, *133*, 16714.
(36) Paulat, F.; Berto, T. C.; DeBeer George, S.; Goodrich, L.; Praneeth, V. K. K.; Sulok, C. D.; Lehnert, N. *Inorg. Chem.* **2008**, *47*, 11449.
(37) Sage, J. T.; Paxson, C.; Wyllie, G. R. A.; Sturhahn, W.; Durbin, S. M.; Champion, P. M.; Alp, E. E.; Scheidt, W. R. *J. Phys.: Condens. Matter* **2001**, *13*, 7707.
(38) Sturhahn, W. *Hyperfine Interact.* **2000**, *125*, 149.
(39) Lin, X. Q.; Kadish, K. M. *Anal. Chem.* **1985**, *57*, 1498.
(40) Frisch, M. J. et al. *Gaussian 03*; Gaussian, Inc.: Pittsburgh, PA, 2003.
(41) Perdew, J. P. *Phys. Rev. B* **1986**, *33*, 8822.
(42) Becke, A. D. *Phys. Rev. A* **1988**, *38*, 3098.
(43) Schaefer, A.; Horn, H.; Ahlrichs, R. *J. Chem. Phys.* **1992**, *97*, 2571.
(44) Schaefer, A.; Huber, C.; Ahlrichs, R. *J. Chem. Phys.* **1994**, *100*, 5829.
(45) Becke, A. D. *J. Chem. Phys.* **1993**, *98*, 1372.
(46) Becke, A. D. *J. Chem. Phys.* **1993**, *98*, 5648.
(47) Neese, F. *ORCA*, 2.2nd ed.; Max-Planck Institut fuer Bioanorganische Chemie: Muelheim/Ruhr, Germany, 2004.
(48) Rose, N. J.; Drago, R. S. *J. Am. Chem. Soc.* **1959**, *81*, 6138.
(49) Beugelskijk, T. J.; Drago, R. S. *J. Am. Chem. Soc.* **1975**, *97*, 6466.
(50) Collman, J. P.; Brauman, J. I.; Doxsee, K. M.; Halbert, T. R.; Hayes, S. E.; Suslick, K. S. *J. Am. Chem. Soc.* **1978**, *100*, 2761.
(51) Wyllie, G. R. A.; Scheidt, W. R. *Chem. Rev.* **2002**, *102*, 1067.
(52) Silvernail, N. J.; Olmstead, M. M.; Noll, B. C.; Scheidt, W. R. *Inorg. Chem.* **2009**, *48*, 971.
(53) Scheidt, W. R.; Barabanschikov, A.; Pavlik, J. W.; Silvernail, N. J.; Sage, J. T. *Inorg. Chem.* **2010**, *49*, 6240.
(54) Scheidt, W. R.; Duval, H. F.; Neal, T. J.; Ellison, M. K. *J. Am. Chem. Soc.* **2000**, *122*, 4651.
(55) Bohle, D. S.; Hung, C.-H. *J. Am. Chem. Soc.* **1995**, *117*, 9584.
(56) Choi, I. K.; Ryan, M. D. *Inorg. Chim. Acta* **1988**, *153*, 25.
(57) Goodrich, L. E.; Paulat, F.; Praneeth, V. K. K.; Lehnert, N. *Inorg. Chem.* **2010**, *49*, 6293.
(58) Praneeth, V. K. K.; Näther, C.; Peters, G.; Lehnert, N. *Inorg. Chem.* **2006**, *45*, 2795.

(59) Praneeth, V. K. K.; Neese, F.; Lehnert, N. *Inorg. Chem.* **2005**, *44*, 2570.
(60) Lehnert, N.; Galinato, M. G. I.; Paulat, F.; Richter-Addo, G. B.; Sturhahn, W.; Xu, N.; Zhao, J. *Inorg. Chem.* **2010**, *49*, 4133.
(61) Lehnert, N.; Sage, J. T.; Silvernail, N. J.; Scheidt, W. R.; Alp, E. E.; Sturhahn, W.; Zhao, J. *Inorg. Chem.* **2010**, *49*, 7197.
(62) Goodrich, L. E.; Lehnert, N. *J. Inorg. Biochem.* **2012**, *118*, 179.
(63) Traylor, T. G.; Sharma, V. S. *Biochemistry* **1992**, *31*, 2847.
(64) Boguslawski, K.; Jacob, C. R.; Reiher, M. *J. Chem. Theory Comput.* **2011**, *2011*, 2740.
(65) Lehnert, N.; Scheidt, W. R.; Wolf, M. W. *Struct. Bonding* **2013**, in press.
(66) Radon, M.; Broclawik, E.; Pierloot, K. *J. Phys. Chem. B* **2010**, *114*, 1518.
(67) Radon, M.; Pierloot, K. *J. Phys. Chem. A* **2008**, *112*, 11824.
(68) Radoul, M.; Sundararajan, M.; Potapov, A.; Riplinger, C.; Neese, F.; Goldfarb, D. *Phys. Chem. Chem. Phys.* **2010**, *12*, 7276.
(69) Zhang, Y.; Gossman, W.; Oldfield, E. *J. Am. Chem. Soc.* **2003**, *125*, 16387.
(70) Neese, F. *J. Chem. Phys.* **2001**, *115*, 11080.
(71) Siegbahn, P. E. M.; Bolmberg, M. R. A.; Chen, S. L. *J. Chem. Theory Comput.* **2010**, *6*, 2040.
(72) Patchkovskii, S.; Ziegler, T. *Inorg. Chem.* **2000**, *39*, 5354.
(73) Radoul, M.; Bykov, D.; Rinaldo, S.; Cutruzzola, F.; Neese, F.; Goldfarb, D. *J. Am. Chem. Soc.* **2011**, *133*, 3043.
(74) Leu, B. M.; Silvernail, N. J.; Zgierski, M. Z.; Wyllie, G. R. A.; Ellison, M. K.; Scheidt, W. R.; Zhao, J.; Sturhahn, W.; Alp, E. E.; Sage, J. T. *Biophys. J.* **2007**, *92*, 3764.
(75) Liu, Y.; Ryan, M. D. *J. Electroanal. Chem.* **1994**, *368*, 209.
(76) Barley, M. H.; Takeuchi, K. J.; Meyer, T. J. *J. Am. Chem. Soc.* **1986**, *108*, 5876.
(77) Barley, M. H.; Rhodes, M. R.; Meyer, T. J. *Inorg. Chem.* **1987**, *26*, 1746.
(78) Dhanasekaran, T.; Grodkowski, J.; Neta, P.; Hambright, P.; Fujita, E. *J. Phys. Chem. A* **1999**, *103*, 7742.
(79) Kadish, K. M.; Shiue, L. R.; Rhodes, R. K.; Bottomley, L. A. *Inorg. Chem.* **1981**, *20*, 1274.
(80) Bartberger, M. D.; Liu, W.; Ford, E.; Miranda, K. M.; Switzer, C.; Fukuto, J. M.; Farmer, P. J.; Wink, D. A.; Houk, K. N. *Proc. Natl. Acad. Sci. U.S.A.* **2002**, *99*, 10958.
(81) Zumft, W. G. *J. Inorg. Biochem.* **2005**, *99*, 194.
(82) Berto, T. C.; Speelman, A.; Zheng, S.; Lehnert, N. *Coord. Chem. Rev.* **2013**, *257*, 244.